

TIME-DELAY FEEDBACK METHODS AND THEIR APPLICATION IN OSCILLATORY SYSTEMS

FARHAN MOHAMMAD HASAN

Doctor of Philosophy

ASTON UNIVERSITY

November 2023

©Farhan Mohamad Hasan, 2023

Farhan Mohammad Hasan asserts his moral right to be identified as the author of this thesis.

This copy of the thesis has been supplied on condition that anyone who consults it is understood to recognise that its copyright rests with its author and that no quotation from the thesis and no information derived from it may be published without appropriate permission or acknowledgement.

Aston University

Time-Delay feedback methods and their application in
oscillatory systems

Farhan Mohammad Hasan

Doctor of Philosophy, November 2023

Reaction-diffusion systems are a paradigm for the study of nonlinear dynamical processes that are taking place in a spatially-extended medium. Examples can be found in many natural systems, ranging from physics and chemistry to biology, and are also applied in areas as different as finances and cultural anthropology. Common aspects of these systems are that they show coherent temporal and spatiotemporal behaviour, reflected by travelling wave solutions, uniform oscillations, spatially periodic but temporally constant patterns (like the famous Turing patterns), or localised patterns like spots. Over the years, the focus of the research of these systems has moved towards the controlling and self-engineering of patterns and systems, notably to the inclusion of feedback loops, designed for stabilising spatiotemporal chaos or inducing novel patterns. These feedback loops can be a consequence of the system dynamics itself (are intrinsic) and are often operating with a time delay since assuming an instantaneous feedback is unrealistic in many cases.

Specifically, in oscillatory reaction-diffusion systems, spatial coupling can render uniform oscillations unstable and can lead to spatiotemporal chaos. The

application of time-delay terms then can stabilize a range of different, including novel, regular solutions. In this thesis, the complex Ginzburg- Landau equation in one-dimensional space subjected to a combined global and local time delayed feedback term has been studied and investigated (a) travelling waves and (b) localized spot patterns. While the travelling wave pattern was found to be transient in simulations, the spot patterns were stable. These patterns are characterized by a change of oscillation amplitude and constant phase shift between the background oscillations and the inside of the localized pattern. The stability area in parameter space, the spatial extension of spots as function of the feedback parameters and the main instabilities has been investigated.

Keywords: Reaction-Diffusion Systems, Nonlinear Oscillations, Complex Ginzburg-Landau Equation, Spatiotemporal chaos, Time-Delay Feedback

To my parents

Acknowledgements

At first, I would like to thank my supervisor Dr. Michael Stich for giving me the opportunity to participate this amazing research work in mathematics. I have learned a lot from his deep knowledge on this subject and broad expertise on numerical analytic field. I would specifically thankful to him for guiding me and helping me to understand and generate brilliant ideas and teaching me any time even in his busiest moments. Without his excellent cooperation and support I wouldn't have reached to the end of my PhD.

Table of Contents

Chapter 1

Introduction	1
1.1 Linear systems.....	2
1.2 Nonlinear systems.....	5
1.3 Oscillations and limit cycles.....	6
1.4 Reaction-diffusion systems and chemical oscillations.....	10
1.5 Complex Ginzburg-Landau Equation.....	12
1.6 Example of a feedback system	16

Chapter 2

Literature review.....	17
------------------------	----

Chapter 3

The complex Ginzburg-Landau Equation.....	29
3.1 Formulations of the CGLE	29
3.2 Numerical Results	35

Chapter 4

Travelling waves	42
4.1 The CGLE with feedback and uniform oscillations	42
4.2 From uniform oscillations to travelling waves	44
4.3 Simulations of transient travelling waves.....	47

Chapter 5

Spot patterns	52
5.1 Model for local feedback	52
5.2 Numerical study of spot patterns	54
5.3 Stability of spot patterns.....	58
5.4 Multiple spot patterns	62

Chapter 6

Final Remarks	67
---------------------	----

References	74
------------------	----

Appendix.....	79
---------------	----

List of figures

Figure 1.1: A linear function	2
Figure 1.2: Limit cycle and Phase Shift.....	8
Figure 1.3: Limit cycle in phase space	9
Figure 1.4: A stable and unstable limit cycle	9
Figure 3.1: Variables vs. Time plot	36
Figure 3.2: Variables vs. Space plot	37
Figure 3.3: Space-time plot of a (stable uniform oscillations)	38
Figure 3.4: Space-time plot of $ A $ (spatial temporal constant oscillations)	39
Figure 3.5: Space-time plot of a (unstable uniform oscillations)	40
Figure 3.6: Space-time plot of $ A $ (irregular spatial temporal oscillations)	40
Figure 3.7: Space-time plot of a (longer simulation time)	41
Figure 3.8: Space-time plot of $ A $ (longer simulation time)	41
Figure 4.1: Sketch of four different wave patterns	46
Figure 4.2: Four different wave patterns	47
Figure 4.3: Short simulations of travelling waves	49
Figure 4.4: Long simulations of travelling waves	50
Figure 4.5: Variables vs. Space of travelling waves.....	51
Figure 5.1: Space-Time plot of 7 types of waves	55
Figure 5.2: Space-Time plot of spot solutions ($t = 50$)	56
Figure 5.3: Space-Time plot of spot solutions ($t = 100$)	57
Figure 5.4: Destabilization of spot solutions	58
Figure 5.5: Stability region for the spot solution	59
Figure 5.6: Spatial size S of a single stable spot solution	61
Figure 5.7: Two spots and grid point analysis	64

List of tables

Table 1.1 Differences between linear and nonlinear waves	15
Table 4.1 Different wave patterns	45

Chapter 1

Introduction

The aim of this thesis is to introduce and investigate a nonlinear chaotic spatially-extended system to which a time-delay feedback can be applied. The purpose of this feedback is to control the dynamic states of the system and to suppress chaos.

As the underlying model system, the complex Ginzburg-Landau equations (CGLE) is used. The CGLE is a standard model for harmonic, nonlinear oscillations in a spatially-extended system, concepts that will be explained in more detail below.

This study is focused on the interplay of global and local feedback terms and their efficiency in suppressing spatiotemporal chaos in a one-dimensional medium. In the focus are the dynamics of spot patterns, i.e. the coexistence of a localized region with non-uniform oscillations with large areas of uniform oscillations, is investigated numerically. Furthermore, travelling waves via numerical simulations has been studied.

This introduction provides a background about what we understand by linear and nonlinear systems, oscillations, and other important concepts.

1.1 Linear systems

What we understand by linear, depends on the context. For example, in calculus, it is a function whose graph is a straight line where the variables are only the first-order polynomial (e.g. $f(x) = mx + n$, where m and n are constant, see Figure 1.1), while in linear algebra it is a linear map (e.g. between two vector spaces).

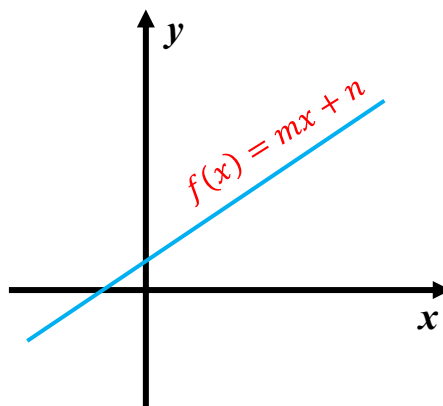


Figure 1.1: A linear function.

In engineering, a linear system is realized when the relationship between input functions x and y and output function f satisfies

$$f(a \cdot x(t) + b \cdot y(t)) = a \cdot f(x(t)) + b \cdot f(y(t)),$$

where a and b are constant real numbers, and x and y are some functions of an independent variable t . In many contexts, the independent variable t of interest represents physical time, but can also refer to other quantities.

Some examples of linear systems and operations in engineering applications [1]:

- Wave propagation; for example – electromagnetic or sound waves
- Electrical circuits build with resistors, capacitors, and inductors
- Electronic circuits; for example – filters or amplifiers
- Mechanical motion that is caused by the interaction of masses, springs, and dashpots/dampeners
- Systems described by specific differential equations; for example – resistor capacitor and inductor networks
- Multiplication by any constant; for example - attenuation or amplification of a signal
- Some specific signal changes; for example – image blurring, resonances, or echoes
- The unity system - where the output is always equal to the input
- The null system - where the output is always zero and not depending on the input
- Differentiation and integration, and the analogous operations of first difference and running for the discrete signal
- Small perturbations in a nonlinear system; for example - a small signal being which is amplified by a properly biased transistor
- Convolution, a mathematical operation where each value in the output is expressed as the sum of values in the input multiplied by the set of weight coefficients
- Recursion, a technique similar to convolution, except previously calculated values in the output are used in addition to values from input

To describe and predict dynamic processes in nature and engineering, differential equations are common [2]. A differential equation $\frac{dy}{dt} = f(t, y)$ is linear if f is linear in y , where y is the dependent variable and t the independent one. For systems of more dependent variables y_1, y_2, \dots, y_n the system of differential equations

$$\frac{dy_1}{dt} = f_1(t, y_1, y_2, \dots, y_n)$$

$$\frac{dy_2}{dt} = f_2(t, y_1, y_2, \dots, y_n) \dots$$

$$\frac{dy_n}{dt} = f_n(t, y_1, y_2, \dots, y_n)$$

is linear if all functions f are linear in all variables y . A dynamical system described by differential equations is linear if the differential equations are linear.

A typical linear system is the ideal, undamped pendulum, which in the case of small angles represents a harmonic oscillator [2]. It can be obtained by linearizing the following nonlinear second-order differential equation

$$\frac{d^2\alpha}{dt^2} + \frac{g}{L} \sin \alpha = 0,$$

where g is the magnitude of the gravitational field, L is the length of the rod of the hanging pendulum, and α is the angle from the vertical to the pendulum.

If the angles from the vertical are considered to be small, then $\sin \alpha \approx \alpha$, and

$$\frac{d^2\alpha}{dt^2} + \frac{g}{L} \alpha = 0,$$

$$\frac{d^2\alpha}{dt^2} + \omega^2 \alpha = 0,$$

where $\omega = \sqrt{\frac{g}{L}}$ is the angular velocity of the oscillation.

The period of oscillations of the undamped pendulum with small angles is therefore

$$T = \frac{2\pi}{\omega} = 2\pi \sqrt{\frac{L}{g}}$$

It is a characteristic of linear oscillations that their frequency does not depend on their amplitude, here, the angle of the pendulum with respect to the vertical.

1.2 Nonlinear systems

In mathematics, a nonlinear function is any function that is not linear. In engineering, a nonlinear system is such a system where the output is not proportional to the changes of the inputs [2]. These systems are present in our nature, such as weather, where its behaviour is chaotic and unpredictable, however, this behaviour is not random. This unpredictability of nature is due to the impossibility to know all variables for all times and that tiny differences in the variables can lead to large differences later (as per a positive Lyapunov exponent), as exemplified by the butterfly effect.

Hence nature and many real applications are nonlinear, justifying why it is an interesting field of study for both scientists and engineers [3].

In mathematics, a differential equation is nonlinear if the dependent variable enters the equation in a nonlinear way (e.g., polynomial of degree higher than one, or a trigonometric function). These equations can be solved analytically sometimes but a general solution cannot be written as a linear combination of particular solutions [2]. Thus, it is common to rely on numerical methods to solve such equations.

Some examples of nonlinear systems in engineering applications [1]:

- Systems which have no static linearity, such as - the voltage and power in a resistor $P = V^2 \cdot R$; the energy emission by radiation of any heated object is $R = k \cdot T^4$ depending on its temperature; the intensity of the light transmitted through a thickness of translucent material $I = e^{-\alpha t}$
- Systems that do not have sinusoidal fidelity such as electronic circuits for peak detection, squaring sine wave to square wave conversion, or frequency doubling
- Common electronic distortion; for example – slewing, crossover distortion, or clipping.
- Multiplication of two signals; for example - in an automatic gain control modulation of amplitude
- Hysteresis phenomena; for example - magnetic flux density versus magnetic intensity in iron or mechanical stress versus strain in vulcanized rubber
- Saturation; for example – transformers and electronic amplifiers driven too hard
- Systems that has a threshold, for example - digital logic gates

1.3 Oscillations and limit cycles

In this thesis, oscillation or oscillatory terminology will appear many times. Oscillation is in principle a temporal phenomenon, which includes periodic and

aperiodic behaviour; within deterministic systems the aperiodic one can be quasiperiodic or chaotic, and can be stochastic, that means that the distribution of amplitudes or other appropriately defined quantities follow a probability distribution. Examples for natural oscillatory systems are the heartbeat and the physiological day-night cycle [2].

We all have an intuitive idea about what oscillations are. In mathematics, an oscillatory function is a function that varies (typically quite often) between its extreme values as it approaches infinity or within a bounded interval. Periodic oscillations can be easily described with amplitude and phase. The amplitude is the value of the function f between the extrema (sometimes also defined as the difference between the extrema, or against a null value). The time interval after which the amplitude values repeat is called the period T . So, we have $f(t) = f(t + T)$ since the values of f repeat, it is customary to define the phase of an oscillation with constant frequency as $\theta = \omega t$ (and identify it with a corresponding value between 0 and 2π). Figure 1.2 illustrates this concept using the FitzHugh-Nagumo model for neuronal dynamics, given by

$$\frac{du}{dt} = u - \frac{u^3}{3} + i,$$

$$\frac{dv}{dt} = (u + a - bv)\varepsilon,$$

where u and v are the variables and the parameters are ε , a , b and i , the input current of the neuron. The time series of variables u and v are shown in the figure 1.2(a) (using parameter values $a = 0.7$, $b = 0.8$, $i = 0.8$, and $\varepsilon = 0.08$, following). The limit cycle oscillations can be seen in $u - v$ space (figure 1.2 (c)). In Fig. 1.2(b), we see the phase defined from (u, v) variables. A related concept is the

phase shift. It defines any change of phase if there is one variable, or the phase difference between two or more variables [2], see Figure 1.2(d).

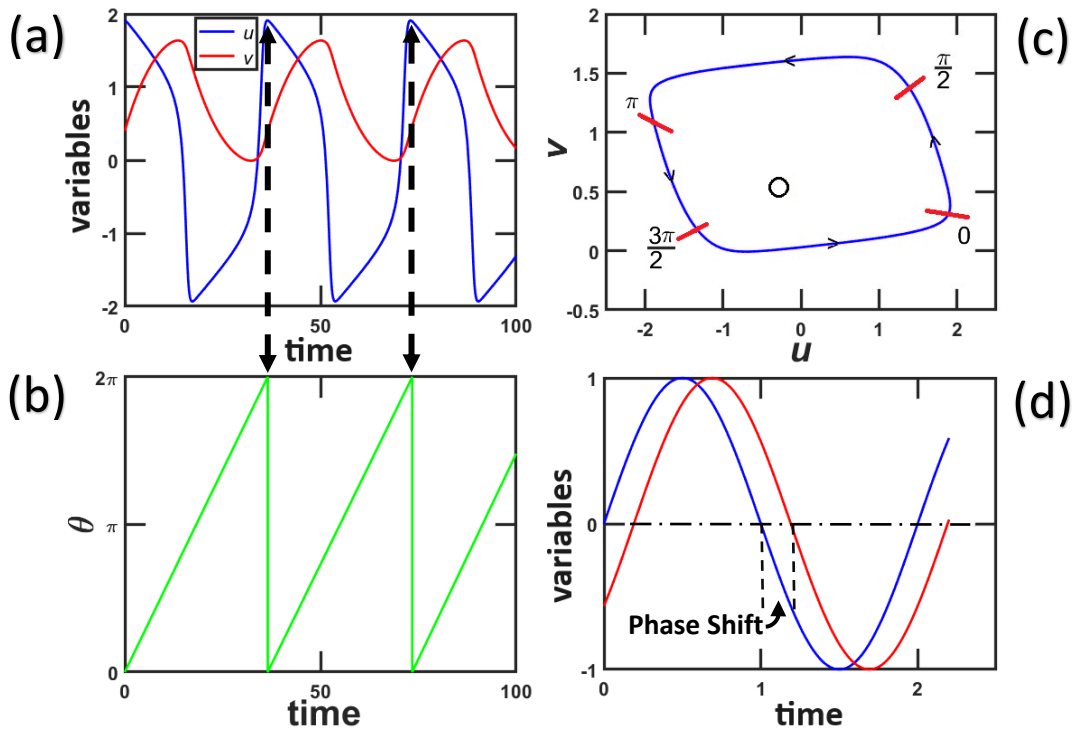


Figure 1.2: (a) Time series of the variables in the oscillatory FitzHugh-Nagumo model. (b) Definition of phase θ from the limit cycle from (a). (c) Blue: limit cycle from (a); red: selected values of the phase (as defined in (b)); open circle: unstable fixed point $(-0.27, 0.53)$ inside the limit cycle. (d) Phase shift (see main text).

Limit cycles represent a sustained, regular oscillation in nonlinear systems. These cycles can be distinguished from linear oscillations because their oscillation amplitude is independent of the initial conditions. A *limit cycle* can be shown in the phase plane as an isolated closed trajectory (or orbit), see Figure 1.3. Typically, a *limit cycle* is shown in phase space defined by the system state variables, so that each variable is assigned to one axis [2].

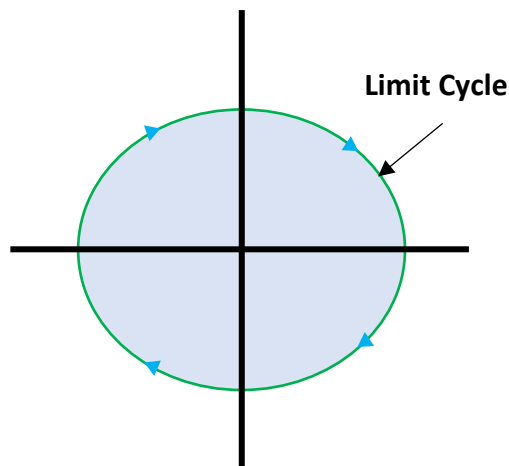


Figure 1.3: Limit cycle in phase space. The arrows on the limit cycle indicate the change of variable. After [5].

Limit cycles can be found, for example, in 2nd order nonlinear systems and have closed orbits or trajectories in phase space (i.e. a space, where every single state of a system is represented, and each possible state of that system corresponds to one unique point). They hold such a property that at least one trajectory spirals into where the time approaches positive infinity or negative infinity. These trajectories are isolated, meaning that neighbouring trajectories are not closed, they either spiral towards or away from the limit cycle. Thus, these closed orbits or trajectories represent stable or unstable solutions of the dynamical system. Self-sustained oscillations are represented by stable limit cycles.

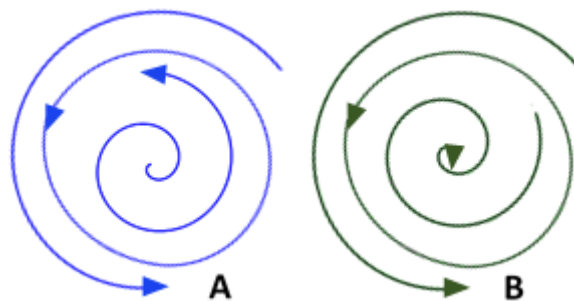


Figure 1.4: A stable limit cycle (A) and an unstable limit cycle (B), after [2]. In case (B), a stable fixed point lies within the limit cycle.

Actually, there are three kinds of limit cycles – (i) stable (ii) unstable and (iii) semi-stable.

- (i) When all trajectories in the proximity of the limit cycle converging to it as $\text{time} \rightarrow \infty$; that means when all neighboring trajectories approach the *limit cycle* as time approaches to positive infinity; then it is *stable limit cycle*.
- (ii) When all trajectories in the proximity of the limit cycle diverging from it as $\text{time} \rightarrow \infty$; that means when all neighboring trajectories approach the limit cycle as time approaches to negative infinity; then it is *unstable limit cycle*.
- (iii) When some trajectories in the proximity of the limit cycle are converging to the limit cycle while others diverging from it as $\text{time} \rightarrow \infty$; then it is *semi-stable limit cycle*.

. Stable and unstable limit cycles are illustrated in Figure 1.4.

1.4 Reaction-diffusion systems and chemical oscillations

Above, I have discussed limit cycles representing temporal oscillations. If the system is spatially-extended (one, two or three dimensions), oscillations can propagate also spatially, producing waves. There is a lot of types of waves that can be observed, a process called *pattern formation*. One typical example for pattern formation within a spatially-extended system occurs when there is perturbation with a nonzero wave number, growing from the spatially uniform state [6]. We may experience these patterns in our everyday life, such as convection

heating system in our houses, where heated air is going up near the radiators, then cooling down, becoming denser and descending due to gravity away from the radiators. If this process repeats, a spatially localised convection cells is formed.

It is not necessary to resort to fluid systems to discuss pattern formation but one can consider a simpler class of models, for example *reaction-diffusion equations* (systems). Thus, I discuss the *diffusion equation* as essential for understanding *reaction-diffusion equations* and oscillatory chemical systems.

According to *Fick's first law*, the diffusion flux is proportional to the spatial gradient of the chemical concentration [7]:

$$J = -D \cdot \nabla c,$$

where J is the *diffusion flux*, D is the diffusion coefficient, c is the concentration.

The continuity equation for mass is:

$$\frac{\partial c}{\partial t} + \nabla \cdot J = 0.$$

Thus, *Fick's second law* (which is the diffusion equation) can be derived, for D being a constant, as:

$$\begin{aligned} \frac{\partial c}{\partial t} + \nabla \cdot (-D \cdot \nabla c) &= 0 \\ \therefore \frac{\partial c}{\partial t} - D \cdot \nabla^2 c &= 0 \\ \therefore \frac{\partial c}{\partial t} &= D \cdot \nabla^2 c \end{aligned}$$

This equation is known as the *diffusion equation*, a parabolic partial differential equation. It is mathematically equivalent to the heat equation for heat transfer. If there are chemical substances which are reacting and diffusing, the *reaction-diffusion equations* can be formed:

$$\partial_t c = f(c) + D \nabla^2 c,$$

where c is the vector of concentrations (it is natural to assume more than one chemical species for reaction systems), f the vector of reaction functions (typically nonlinear), and D the diffusion matrix.

Oscillations in chemical systems have intrigued people for a long time [8]. In 1828, G.T. Fechner first reported a chemical oscillatory system. Later, W. Ostwald observed an inhomogeneous reaction during chromium dissolution rate in acid, and an increase or decrease of the periodic oscillation of the chemical reaction process. At the beginning of the 20th century, it was believed that oscillations are not possible in homogenous reaction systems. In the 1950s, Belousov observed that in the Krebs (citric acid) cycle reactions (cerium as a catalyst and citric acid as reductant) the solution oscillates between two visually distinguishable states, transparent and yellow. However, as the temperature rises, the oscillation frequency increases. His observation proved that the oscillations between colours changes in the solution occurs due to the concentration of cerium, in other words, oscillations in a homogenous reaction are possible. Afterwards, this Belousov-Zhabotinsky reaction has been studied in much detail and is now a paradigm for oscillating reaction-diffusion systems.

1.5 Complex Ginzburg-Landau Equation

The complex Ginzburg-Landau equation (CGLE) is one of the vast researched nonlinear equations. It describes a wide range of phenomena, from nonlinear waves in reaction-diffusion systems to second-order phase transitions, superconductivity, etc. [9].

The CGLE describes the dynamics of isotropic spatially-extended systems near the threshold of a supercritical Hopf instability, leading to uniform oscillations. Near threshold, the equations are universal and can be written in terms of complex amplitudes of the most unstable oscillatory mode [9]. Therefore, it describes nonlinear oscillations. It reads

$$\partial_t A = (1 - i\omega)A - (1 + i\alpha)|A|^2 A + (1 + i\beta)\nabla^2 A$$

where, A = complex oscillation amplitude
 ω = linear frequency parameter
 α = nonlinear frequency parameter
 β = linear dispersion coefficient

Due to the presence of the Laplacian $\nabla^2 A$, this equation can be interpreted as a nonlinear reaction-diffusion equation, $\partial_t A = f(A) + D\nabla^2 A$, where f is a nonlinear function. The presence of the Laplacian operator characterizes dissipative processes, like diffusion of chemical substances or the dissipation of heat. Since A is a complex variable, it can be interpreted mathematically as two reaction-diffusion equations for two real variables. It can be shown that the CGLE is the normal form of a supercritical Hopf bifurcation in a spatially extended system, i.e., even if the original reaction-diffusion system has n variables, its dynamics is described by only two variables, and which then can be represented by A .

Oscillations in the CGLE can be described in terms of amplitude and phase or frequency. This can be written as $A = \rho e^{-i\Omega t}$, or $A = \rho e^{i\Omega t}$, where A = complex variable (complex amplitude), t = time, ρ = real amplitude (modulus of A), Ω = frequency. The product Ωt is the phase of the oscillation.

Nonlinear dissipative media, as modelled by the CGLE, not only show temporally periodic behaviour but also display spatiotemporally disordered, chaotic

states [9]. Since the CGLE represents a reaction-diffusion system, spatiotemporal chaos can be created by the diffusion part and is observed if the parameter inequality $1 + \alpha\beta < 0$ is fulfilled (the Benjamin-Feir or Benjamin-Feir-Newell criterion). In order to influence the system dynamics, it has been found that reaction-diffusion systems can be controlled and engineered by external force and internal feedback signals [10], following fundamental work on controlling chaos by Ott, Grebogi and Yorke [11].

Furthermore, spatiotemporal chaos can be controlled by feeding back a global time-delayed signal into the system [10]. This method is also known as time-delay auto-synchronization (TDAS) which was first proposed by Pyragas in 1992 [12]. In TDAS, a feedback signal such as F can be applied which is proportional to the difference between the actual state of the system and its delayed one. For controlling the feedback in such systems two types of control can be considered: (i) global and (ii) local control.

This thesis represents further investigation of this approach, based on the CGLE with a time-delay auto-synchronization (TDAS) feedback with local and global contributions, first presented in [13]:

$$\frac{\partial A}{\partial t} = (1 - i\omega)A - (1 + i\alpha)|A|^2A + (1 + i\beta)\frac{\partial^2 A}{\partial x^2} + F$$

where A = complex oscillation amplitude

ω = linear frequency parameter

α = nonlinear frequency parameter

β = linear dispersion coefficient

F = feedback term

$$F = \mu \cdot e^{i\xi} \cdot [m_l \{A(x, t - \tau) - A(x, t)\} + m_g \{\bar{A}(t - \tau) - \bar{A}(t)\}],$$

where μ = feedback strength

ξ = phase shift

τ = delay time

m_g = global feedback strength

m_l = local feedback strength

and
$$\bar{A}(t) = \frac{1}{L} \int_0^L A(x, t) dx$$

where, \bar{A} = spatial average

L = one-dimensional system length

In the literature review, I discuss previous results of this and related models in detail. The table below gives schematically some differences between linear and nonlinear waves, in the spirit of the differences between linear and nonlinear systems as described above.

Table 1.1 Differences between linear and nonlinear waves

Linear wave	Nonlinear wave
Frequency does not depend on the amplitude	Frequency depends on the amplitude
Amplitude does not depend on the wave number	Amplitude depends on the wave number
Waves decay due to dissipation	Waves do not decay, system is active, consumes energy
Waves do not interact; linear superposition applies	Waves interact; nonlinear collisions and shocks
No frequency selection	Topological defects and boundaries select unique frequency

1.6 Example of a feedback system

One example of a time-delayed feedback system is to control chaos in current-controlled power converters in a power generation system [43].

Let us consider this example in more detail. A power generation system which generates varied voltage, for example photovoltaic (PV) cells, needs a DC-DC boost converter to work as an intermediate power processing unit that connects the power generation system with the load. Internally, such converters work as a periodic process for the induction current of the circuit. However, DC-DC boost converters are a type of power converters which may reach nonlinear operating conditions when they are connected to a power generation which varies due to environmental conditions (e.g. irradiation or temperature) [44].

While every power converter is designed to work within its operating region as a stable process, beyond its operating region it may face limitations or instabilities. In this case, the induction current undergoes period-doubling bifurcations as the reference current is increased, leading to a chaotic time series of the induction current [36]. In practice, this means not only unpredictability of the current but also that so-called noise ripples may lead to crash the converter [43]. Therefore, in order to keep the converter its periodic operation, the chaotic states in any form should be avoided and it is essential to control these chaotic states in this specific nonlinear system. By using a time-delay feedback term $K[i_L(t - \tau) - i_L(t)]$, where K is the feedback strength, τ the delay time and i_L the induction current of the circuit, the authors are able to induce a periodic operation of the otherwise chaotic DC-DC boost converter.

Chapter 2

Literature review

This thesis builds on a range of previous research. Specifically, I review relevant publications in nonlinear oscillations and their control.

In the context of nonlinear oscillations, the complex Ginzburg-Landau equation (CGLE) is one of the most studied equations [9]. This equation can be interpreted as a reaction-diffusion equation and as such can have purely temporal or spatiotemporal solutions. The basic solution of the CGLE represents uniform oscillations, but depending on the system parameters, these uniform oscillations may be stable or unstable. Different regular states (for example, plane waves or Bekki-Nozaki holes) are solutions, but also phase and amplitude turbulence, examples for spatiotemporal chaos, are possible [9]. This equation will be discussed more in the Chapter 3.

It is of interest to control chaotic states. Following the pioneering work by Ott, Grebogi and Yorke to control chaos in non-spatial systems [11], Pyragas showed in 1992 that spatiotemporal chaos can be controlled by feeding back a global time-delayed signal to the system [12]. This method is also known as time-delay auto-synchronization (TDAS). In TDAS, a feedback signal, say F , can be applied which is proportional to the difference between the actual state of the system (such as $A(t)$) at any given time (i.e. t) and the state of the system before

(i.e. $t - \tau$). This proportionality can be expressed as $F(t, \tau) \propto A(t - \tau) - A(t)$. The research presented in this work is based on a feedback term of this kind.

In the context of the CGLE, control of spatiotemporal chaos via global feedback has first been investigated in 1996 by Battogtokh and Mikhailov [14]. They have used time delay to vary the phase shift between global control signal and average oscillation phase in the medium [14]. Thus, by adjusting the delay time and the phase shift they have characterized the condition to obtain uniform oscillations [14]. This research is relevant for the present work as in this work global feedback terms within the CGLE are used as well, although I include furthermore local terms.

A further investigation [15] focussed on controlling spatiotemporal chaos using time-delay feedback control (described below) by providing a transition from travelling waves to stationary periodic patterns. The authors observed, when the time-delay feedback control was applied to travelling pluses within the Gray-Scott model two possible final states were found. After implementing activator and inhibitor control into the system, wave splitting and spatially periodic Turing pattern has been observed. This method shows how spatiotemporal chaos in the Gray-Scott model can be controlled [15]. While that work was made for a model fundamentally different from the one studied in this thesis (see in particular Chapter 4), it provides a successful example for feedback control in reaction-diffusion systems.

In 2002, a comparison of time delay control methods for stabilizing several solutions had been published, where a generic reaction-diffusion system with global coupling was considered [16]. The results of this paper have some similarity with the results and discussion in Chapter 4, however in this work, both local and

global terms have been introduced, and also the underlying model (the CGLE) is different from the [16].

In 2004, Beta and Mikhailov used a global TDAS scheme to control spatiotemporal chaos in the CGLE [17]. It has been found that a non-invasive stabilization of uniform oscillations cannot be possible if the CGLE is in the Benjamin-Feir unstable regime, although the feedback signal could be reduced to a minimum. This study also analysed the stability of uniform oscillations as function of the feedback parameters, in particular long delay times [17]. In Chapter 4 and 5, I will be showing some results on short and long time-delays that have similarities of this paper. Again, the presence of local terms in the main difference to [17].

Afterwards, Stich, Casal and Beta introduced a combination of *global* and *local* control into TDAS to control spatiotemporal chaos in the CGLE [13]. The resulting model (the equations were already shown in Chapter 1) is the framework of the system developed in this thesis and therefore it is of interest to describe the behaviour of this model in more detail. In the first place, appropriate feedback strengths and delay times can induce uniform oscillations for a variety of weights of local vs. global terms. Not only uniform oscillations are described: For stable and perfectly regular standing waves, a combination of local and global TDAS terms is important [13]. In the same article, it also has been observed that the presence of local TDAS terms prevents uniform oscillations to be stabilized and helps to form spatiotemporal patterns which for purely global TDAS would be either non-existing, or unstable [13]. That publication is the basis of part of the present research, in particular for travelling waves.

In follow-up work, Stich and Beta, a linear stability analysis of uniform oscillations with respect to spatiotemporal perturbations (perturbations of a given wavenumber) was performed [18]. In this way, they could characterize the standing waves as an instability of uniform oscillations with respect to waves with a certain wavenumber [18]. Therefore, standing waves appear in parameter areas adjacent to regions where stable uniform oscillations are observed. They also discussed multi-stability of uniform oscillations and therefore hysteresis effects [18]. Another solution that had been discussed is the so-called amplitude death, favoured for high local (and low global) contributions to the feedback [18]. Amplitude death indicates the transition from an oscillatory solution to a stationary fixed point. In this system, amplitude death can be stabilized non-invasively [18]. A stability analysis for the models studied in Chapters 4 and 5 is a formidable task to do, however, is left for further work.

In subsequent work, standing waves were analysed in more detail, in particular their instabilities were described, for example the instability to a breathing mode [19]. Another aspect of that model has been described in a different publication, focusing on multi-stability of solutions and the fact that the fundamental equations become delay differential equations and more results rely on numerical evaluation [19]. In that work, different values of the phase shift parameter ξ (i.e., 0 to 2π) have been considered instead of one fixed value (e.g., $\frac{\pi}{2}$), as in [13, 18, 19]. It has been also reported in that work that, for global feedback, the amplitude death cannot happen when local feedback is zero [20]. In all the present work presented here, the value ξ is chosen to be $\frac{\pi}{2}$ for consistency with the mentioned articles.

In further work [21], the pattern formation in that model was investigated under the influence of noise, in particular with respect to standing waves: it has been observed that in the small noise does not destabilize deterministically stable standing waves and that in the deterministically unstable regime, but close to the boundary, a small noise intensity can induce standing waves [21]. Their work has some similarity to the present research as unstable regimes will be also reported in Chapter 4 and 5.

The CGLE also been implemented to investigate travelling waves with feedback. By using linear stability analysis, Montgomery and Silber [22] have found for the one-dimensional CGLE in the Benjamin-Feir unstable regime travelling wave solutions in a non-invasive feedback control scheme can be stabilized. Using a stability analysis, the authors find an optimal value of one of the feedback parameters to determines whether a travelling wave is stable to all perturbation wavenumbers [22]. This is one of the few published works on travelling waves. However, the feedback scheme is essentially different and particularly designed for wave control, unlike the model studied in Chapter 4.

Another investigation, by Postlethwaite and Silber [23], was conducted on travelling waves for two-dimensional CGLE in a spatial and temporal feedback control system, similar to the control system studied earlier [22]. In the present study, space is one-dimensional and, therefore, the mentioned publication has no direct impact on this work. However, together with [22] it gives a glance on what features could be found once the dimensionality of the system changes.

I should also mention research on other models with have some resemblance with my model. Another research for the CGLE [24] was done to drive

a spatiotemporal chaotic state into stable plane wave solutions via a set of local controllers of Pyragas type. Their model is

$$\dot{A} = A + (1 + i\alpha)\partial_x^2 A - (1 + i\beta)|A|^2 A + U(x, t)$$

with $U(x, t) = 0$ for $x \neq x_i$

and $U(x, t) = K_0\{g(x_i, t) - A(x_i, t)\}$ for $x = x_i$

where $i = 1, 2, \dots, M$ and $x_i = 1 + (i - 1)\nu$ are the positions of M local, equally spaced controllers, mutually separated by a distance ν , i.e.,

$$x_{i+1} - x_i = \nu.$$

The function $g(x)$ is the plane wave solution

$$g(x, t) = \sqrt{1 - q^2} e^{i(qx + \omega t)}, \text{ for } -1 \leq q \leq 1$$

The main result is that they achieve the control of the spatiotemporal chaos and induce plane waves, when large enough control strengths and density of controllers (M large enough) has been used.

Research done in 2017 [25] derived some general criteria for the stabilization of solutions for the CGLE by using different kind of feedback control algorithms (on the right-hand side of the following equations). Their models read

$$u_t - (\lambda + i\alpha)u_{xx} + (\kappa + i\beta)|u|^p u - \gamma u = -\mu \sum_{k=1}^N \bar{u} \chi_{jk}(x)$$

and

$$u_t - (\lambda + i\alpha)\Delta u + (\kappa + i\beta)|u|^p u - \gamma u = -\mu \sum_{k=1}^N (u, \omega_k) \omega_k$$

complemented by suitable Neumann and Dirichlet boundary conditions.

The first feedback term represents a locally averaged (over N intervals) feedback, and the second one N Fourier modes (for further details about the meaning of the notation in the feedback terms, see [25]). My models, adapted to their notation, have $\lambda = 1$, $\kappa = 1$, $\gamma = 1$ and $p = 2$, while they do not have terms corresponding to χ or to ω . Moreover, the feedback terms themselves are fundamentally different, so a comparison of [25] to the model used in this work cannot be made.

Another research [26] has investigated the dynamics near a resonant double *Hopf bifurcation* in a CGLE with local feedback, written (in my notation)

$$\begin{aligned} \frac{\partial A(x, t)}{\partial t} = & \frac{\partial^2 A(x, t)}{\partial x^2} + [(1 + i\omega) - (1 + i\alpha)|A(x, t)|^2]A(x, t) \\ & + \mu e^{-i\xi}[A(x, t - \tau) - A(x, t)] \end{aligned}$$

The main difference to the model in this thesis is that there is no parameter β (or, which is the same, $\beta = 0$) and therefore the system dynamics they consider is always *Benjamin-Feir-Newell stable*, and no spatiotemporal chaos is observed. Furthermore, they only have what is generally known as local feedback, since no spatially-averaged (*global*) term is present in their model. As a result of these differences, the authors of [26] consider a different bifurcation that occurs in the model, the *resonant double Hopf-bifurcation*, (which is, a double Hopf-bifurcation where there is at bifurcation an integer relation between the imaginary eigenvalues, or imaginary Floquet exponents) and the system dynamics cannot be compared easily.

In their study [27] from 2023, Tzou and Xie showed how localized structures (spots) interact and how their collective dynamics can lead to oscillatory behaviour.

They had an asymptotic analysis that deals with the stability of N-spot equilibrium solutions to the Schnakenberg reaction-diffusion system. The analysis leads to the formulation of a $2N \times 2N$ complex matrix eigenvalue problem. This matrix captures the essential dynamics of the system near the Hopf bifurcation threshold. This suggests a relationship between the steady-state patterns in the reaction-diffusion system and solutions to optimization problems where certain configurations minimize or optimize some criterion related to escape or diffusion. This paper was about single spot patterns and simple geometries, however in chapter 5 I have shown some results with multi-spot patterns in one-dimensional domains.

A study [28] by Nishiura and Xie provides a detailed analysis of the dynamics of localized spots in a three-component reaction-diffusion system, focusing on the formation and movement of ring patterns. For their study they system they have considered is - N-spot bound state with three-component (u_t, v_t, θ_t) reaction-diffusion system, see more details in [28]. By reducing the system to a set of ODEs and validating the results with numerical simulations, the research offers significant insights into pattern formation and collective motion. They have shown that ring patterns emerge as fundamental structures within reaction-diffusion systems, serving as the basis for understanding more intricate pattern formation and dynamics. Their research opened the scope to higher-order interactions (i.e., the simulation of seven-spot ring patterns) of new spots pattern formation in more complex and realistic scenarios. In chapter 5, I have shown multi-spot patterns within one-dimensional domain, however the dynamics are very different.

In 2003, [29] Yang and Epstein investigated a model of reaction-diffusion system with two coupled layers presents a case of pattern formation, where the

interaction between oscillatory and stationary dynamics leads to unique and intricate patterns. The observed *twinkling eyes* and localized spiral or concentric waves demonstrate the rich variety of structures that can emerge from such systems. This research not only enhances our understanding of reaction-diffusion systems but also has broader implications for studying similar phenomena in natural and synthetic systems. In their proposed model of a reaction-diffusion system with two coupled layers offers significant insights into the formation of novel oscillatory Turing patterns. The spontaneous formation of these patterns, such as twinkling eyes, localized spirals and concentric waves, and pinwheels, demonstrates the complexity that can arise from simple interactions between different dynamical modes. Although the pattern looks quite similar to a multi-spot pattern as studied in Chapter 5, the underlying dynamics is quite different as there is not Turing instability in the system studied there.

In 2021 [30] Al Saadi et. al. investigates simple predator-prey models with rational interaction terms in both one-dimensional and two-dimensional spatial domains. They found that the pattern formation in predator-prey models with rational interaction terms and saturation. The analysis reveals the conditions under which localized and complex spatio-temporal patterns emerge, driven by subcritical Turing bifurcations and Hopf bifurcations. Unlike Schnakenberg type models, predator-prey systems can undergo Hopf bifurcations in addition to Turing instabilities. In this studied predator-prey models, parameter regimes with subcritical Turing bifurcations can lead to localized patterns even without spatially heterogeneous causes. While the primary focus of the paper is not on practical applications in spatial ecology, the findings have broad implications for understanding spatially localized patterns in ecological systems. The observation

that localized patterns can arise without spatially heterogeneous causes challenges conventional assumptions and highlights the importance of considering the underlying mechanisms, such as subcritical Turing bifurcations, in ecological modeling. In chapter 5, I have shown multi-spot patterns which have different dynamics from this study.

Another work [31] was presented by T. Ohta in 2001, where the study formulates a theory for pulse dynamics in an excitable reaction-diffusion system, extending the analysis from one dimension to higher dimensions. Specifically, it investigates the behavior of interacting pulses, which represent localized excitation fronts in the system. The derived equation of motion for interacting pulses (spots in higher dimensions) reveals a bifurcation phenomenon and the emergence of an inertia term, shedding light on the role of delayed interactions in shaping pulse propagation dynamics. The study emphasizes the justification and internal consistency of the theoretical framework for analyzing pulse dynamics in excitable reaction-diffusion systems. By aligning the assumptions with the conditions under which reflection phenomena occur, the theory maintains coherence and applicability within the defined parameter regime.

In nonlinear dissipative systems, such as reaction-diffusion media, a translational bifurcation is a critical phenomenon that significantly influences the behavior of domain boundaries. In 1996, Ohta and Kiyose's investigation [32] confirms that translational bifurcation plays a critical role in the elastic-like collision of domain boundaries in nonlinear dissipative systems. By incorporating inertia, damping, and interaction terms in the interface equation, the framework provides a robust approach to understanding and predicting these phenomena across various reaction-diffusion systems. They have shown that the translational

bifurcation (at positive constant τ) is crucial for enabling elastic-like collisions of domain boundaries in a Bonhoffer-van der Pol type reaction-diffusion system. Their theoretical analysis based on interface dynamics and simulations confirms that such behavior is only observed within a restricted parameter region due to the specific requirements for degeneracy in direction and small velocity near the bifurcation point. This comprehensive approach provides a deep understanding of the conditions under which elastic-like collisions can occur. The dynamics of their system is not oscillatory and they have observed phenomenon like breathing and disappearing spots, which has some similarity of my current work where I have found spots in oscillatory system, which I will be describing more in Chapter 5.

In 2000, Muratov and Osipov published their study [33] on static spike autosolitons in the Gray–Scott model involves asymptotic analysis and matching of inner and outer solutions. These structures exist over a wide range of parameters in one dimension and a narrower range in higher dimensions. They did asymptotic analysis of the Gray-Scott model which reveals that static spike autosolitons exist in regions where the characteristic length scales of the activator and inhibitor are significantly different. These solutions are characterized by narrow spikes in the concentration of the activator substance. These static spike autosolitons exhibit varying stability and existence ranges depending on the spatial dimension. In one dimension, these structures exist over a wide range of parameters and are stable. This behaviour can be typical in reaction-diffusion systems where the balance between local reaction kinetics and diffusion leads to the formation of stable, localized structures. At a critical value of a bifurcation point the stable spike autosolitons disappear. The abrupt disappearance or splitting at bifurcation parameter point are indicative of underlying nonlinear dynamics and

bifurcation phenomena, which are key aspects in the study of spot pattern formation and nonlinear wave theory. In Chapter 5, I have showed one dimensional spot patterns in different dynamics.

Chapter 3

The complex Ginzburg-Landau Equation

In this chapter, I state some basic results for the complex Ginzburg-Landau equation without time-delay feedback. The CGLE is a complex equation for the complex variable A . It therefore can be formulated with real part a and imaginary part b or with amplitude ρ and phase φ . I give both formulations below. I give the criterion on spatiotemporal chaos and the solution of uniform oscillations and accompany this with numerical simulations. These results are not novel, but they are the foundations for the remainder of this thesis.

3.1 Formulations of the CGLE

Real and imaginary parts of the CGLE

Let's start with the standard formulation of the CGLE:

$$\frac{\partial A}{\partial t} = (1 - i\omega)A - (1 + i\alpha)|A|^2A + (1 + i\beta)\nabla^2 A \quad (3.1)$$

Now, use $A = a + ib$ to express the left-hand side (LHS) and the terms on the right-hand side (RHS) as sum of real and imaginary terms:

$$\text{LHS} = \frac{\partial A}{\partial t} = \frac{\partial(a+ib)}{\partial t} = \frac{\partial a}{\partial t} + i \frac{\partial b}{\partial t}$$

On the RHS, the non-spatial terms of the CGLE are considered first:

$$\begin{aligned}
\text{RHS 1} &= (1 - i\omega)(a + ib) - (1 + i\alpha)|a + ib|^2(a + ib) \\
&= (a + ib - i\omega a + \omega b) - (a + ib + i\alpha a - \alpha b)|a + ib|^2 \\
&= (a + ib - i\omega a + \omega b) - (a + ib + i\alpha a - \alpha b)(a^2 + b^2) \\
&= (a + ib - i\omega a + \omega b) - (a^3 + ia^2b + i\alpha a^3 - \alpha a^2b + ab^2 + ib^3 + i\alpha ab^2 - \alpha b^3) \\
&= a + ib - i\omega a + \omega b - a^3 - ia^2b - i\alpha a^3 + \alpha a^2b - ab^2 - ib^3 - i\alpha ab^2 + \alpha b^3 \\
&= \{a - a^3 - ab^2 + \omega b + \alpha a^2b + \alpha b^3\} + i\{b - a^2b - b^3 - \omega a - \alpha a^3 - \alpha ab^2\} \\
&= [a\{1 - (a^2 + b^2)\} + b(\omega + \alpha(a^2 + b^2))] + i\{b\{1 - (a^2 + b^2)\} - a(\omega + \alpha(a^2 + b^2))\}
\end{aligned}$$

Now, the spatial terms have to be considered, assuming one-dimensional space:

$$\begin{aligned}
\text{RHS 2} &= (1 + i\beta)\nabla^2 A \\
&= (1 + i\beta)\nabla^2(a + ib) \\
&= (1 + i\beta)\left\{\frac{\partial^2 a}{\partial x^2} + i\frac{\partial^2 b}{\partial x^2}\right\} \\
&= \frac{\partial^2 a}{\partial x^2} + i\frac{\partial^2 b}{\partial x^2} + i\beta\frac{\partial^2 a}{\partial x^2} - \beta\frac{\partial^2 b}{\partial x^2} \\
&= \frac{\partial^2 a}{\partial x^2} - \beta\frac{\partial^2 b}{\partial x^2} + i\left\{\beta\frac{\partial^2 a}{\partial x^2} + \frac{\partial^2 b}{\partial x^2}\right\} \\
&= \frac{\partial^2}{\partial x^2}(a - \beta b) + i\frac{\partial^2}{\partial x^2}(\beta a + b)
\end{aligned}$$

I collect all terms and then I separate real and imaginary parts for the RHS and

LHS:

Real Part:

$$\frac{\partial a}{\partial t} = a\{1 - (a^2 + b^2)\} + b\{\omega + \alpha(a^2 + b^2)\} + \frac{\partial^2}{\partial x^2}(a - \beta b) \quad (3.2)$$

Imaginary Part:

$$\frac{\partial b}{\partial t} = b\{1 - (a^2 + b^2)\} - a\{\omega + \alpha(a^2 + b^2)\} + \frac{\partial^2}{\partial x^2}(\beta a + b) \quad (3.3)$$

By combining the spatial and non-spatial parts, two new equations (3.2 and 3.3) have been obtained. These two equations are equivalent to the CGLE in complex notation (3.1), having used $A = a + ib$. It is this formulation in real and imaginary parts which is used to find the numerical solutions of the CGLE using the Euler method for the non-spatial part, and a 3-point representation of the Laplacian for the spatial part.

For solving an *ordinary differential equation* (ODE) with any given initial value, the Euler method can be used. It is the simplest, first-order, explicit method (i.e., it directly calculates the state of a system at a later time from the state of the system at the current time) for numerical integration of ODEs.

Amplitude and phase representation of the CGLE

Now I use the amplitude-phase representation of complex numbers, $A = \rho e^{-i\varphi}$, to express the CGLE, separating again into left-hand side (LHS) and right-hand side (RHS):

$$\begin{aligned}
 \text{LHS} &= \frac{\partial A}{\partial t} = \frac{\partial(\rho e^{-i\varphi})}{\partial t} \\
 &= \rho \frac{\partial}{\partial t} e^{-i\varphi} + e^{-i\varphi} \frac{\partial}{\partial t} \rho \\
 &= \rho \cdot (-ie^{-i\varphi}) \cdot \frac{\partial \varphi}{\partial t} + e^{-i\varphi} \frac{\partial \rho}{\partial t} \\
 &= e^{-i\varphi} \cdot \frac{\partial \rho}{\partial t} - ie^{-i\varphi} \cdot \rho \frac{\partial \varphi}{\partial t} \\
 &= e^{-i\varphi} \left[\frac{\partial \rho}{\partial t} - i\rho \cdot \frac{\partial \varphi}{\partial t} \right]
 \end{aligned}$$

On the RHS, the non-spatial terms of the CGLE are considered first:

$$\begin{aligned}
 \text{RHS 1} &= (1 - i\omega)(\rho e^{-i\varphi}) - (1 + i\alpha)|\rho e^{-i\varphi}|^2(\rho e^{-i\varphi}) \\
 &= (1 - i\omega)(\rho e^{-i\varphi}) - (1 + i\alpha) \cdot \rho^2 \cdot 1 \cdot (\rho e^{-i\varphi}) \\
 &= e^{-i\varphi}[\rho - i\omega\rho - \rho^3 - i\alpha\rho^3] \\
 &= e^{-i\varphi}[(\rho - \rho^3) - i(\omega\rho + \alpha\rho^3)] \\
 &= e^{-i\varphi}[\rho(1 - \rho^2) - i\rho(\omega + \alpha\rho^2)]
 \end{aligned}$$

Now, the spatial terms must be considered, assuming one-dimensional space:

$$\begin{aligned}
 \text{RHS 2} &= (1 + i\beta)\nabla^2(\rho e^{-i\varphi}) \\
 &= (1 + i\beta)\frac{\partial^2}{\partial x^2}(\rho e^{-i\varphi}) \\
 &= (1 + i\beta)\left[\frac{\partial}{\partial x}\frac{\partial}{\partial x}(\rho e^{-i\varphi})\right] \\
 &= (1 + i\beta)\left[\frac{\partial}{\partial x}\left\{\rho\frac{\partial}{\partial x}e^{-i\varphi} + e^{-i\varphi}\frac{\partial\rho}{\partial x}\right\}\right] \\
 &= (1 + i\beta)\left[\frac{\partial}{\partial x}\left\{\rho \cdot (-ie^{-i\varphi}) \cdot \frac{\partial\varphi}{\partial x} + e^{-i\varphi}\frac{\partial\rho}{\partial x}\right\}\right] \\
 &= (1 + i\beta)\left[\left\{\rho \cdot (-ie^{-i\varphi})\right\} \cdot \frac{\partial^2\varphi}{\partial x^2} + \frac{\partial\varphi}{\partial x} \cdot \frac{\partial}{\partial x}\left\{\rho \cdot (-ie^{-i\varphi})\right\} + e^{-i\varphi} \cdot \frac{\partial^2\rho}{\partial x^2} + \frac{\partial\rho}{\partial x} \cdot \frac{\partial}{\partial x}(e^{-i\varphi})\right] \\
 &= (1 + i\beta)\left[\left\{\rho \cdot (-ie^{-i\varphi})\right\} \cdot \frac{\partial^2\varphi}{\partial x^2} + \frac{\partial\varphi}{\partial x} \cdot \left\{\rho\frac{\partial}{\partial x}(-ie^{-i\varphi}) + (-ie^{-i\varphi})\frac{\partial\rho}{\partial x}\right\} + e^{-i\varphi} \cdot \left[\frac{\partial^2\rho}{\partial x^2} + \frac{\partial\rho}{\partial x} \cdot (-ie^{-i\varphi}) \cdot \frac{\partial\varphi}{\partial x}\right]\right] \\
 &= (1 + i\beta)\left[\left\{\rho \cdot (-ie^{-i\varphi})\right\} \cdot \frac{\partial^2\varphi}{\partial x^2} + \frac{\partial\varphi}{\partial x} \cdot \left\{\rho \cdot -i\frac{\partial}{\partial x}(e^{-i\varphi}) + (-ie^{-i\varphi})\frac{\partial\rho}{\partial x}\right\} + e^{-i\varphi} \cdot \left[\frac{\partial^2\rho}{\partial x^2} + \frac{\partial\rho}{\partial x} \cdot (-ie^{-i\varphi}) \cdot \frac{\partial\varphi}{\partial x}\right]\right] \\
 &= (1 + i\beta)\left[-i\rho e^{-i\varphi}\frac{\partial^2\varphi}{\partial x^2} - i\rho\frac{\partial\varphi}{\partial x} \cdot (-ie^{-i\varphi}\frac{\partial\varphi}{\partial x}) - ie^{-i\varphi}\frac{\partial\varphi}{\partial x}\frac{\partial\rho}{\partial x} + e^{-i\varphi}\frac{\partial^2\rho}{\partial x^2} - ie^{-i\varphi}\frac{\partial\rho}{\partial x}\frac{\partial\varphi}{\partial x}\right]
 \end{aligned}$$

$$\begin{aligned}
&= (1 + i\beta) \left[-i\rho e^{-i\phi} \frac{\partial^2 \varphi}{\partial x^2} - \rho \frac{\partial \varphi}{\partial x} \cdot \left(e^{-i\phi} \frac{\partial \varphi}{\partial x} \right) - 2i e^{-i\phi} \frac{\partial \varphi}{\partial x} \frac{\partial \rho}{\partial x} + e^{-i\phi} \frac{\partial^2 \rho}{\partial x^2} \right] \\
&= (1 + i\beta) e^{-i\phi} \left[-i\rho \frac{\partial^2 \varphi}{\partial x^2} - \rho \frac{\partial \varphi}{\partial x} \cdot \left(\frac{\partial \varphi}{\partial x} \right) - 2i \frac{\partial \varphi}{\partial x} \frac{\partial \rho}{\partial x} + \frac{\partial^2 \rho}{\partial x^2} \right] \\
&= e^{-i\phi} \left[-i\rho \frac{\partial^2 \varphi}{\partial x^2} - \rho \left(\frac{\partial \varphi}{\partial x} \right)^2 - 2i \frac{\partial \varphi}{\partial x} \frac{\partial \rho}{\partial x} + \frac{\partial^2 \rho}{\partial x^2} + \beta \rho \frac{\partial^2 \varphi}{\partial x^2} - i\beta \rho \left(\frac{\partial \varphi}{\partial x} \right)^2 + 2\beta \frac{\partial \varphi}{\partial x} \frac{\partial \rho}{\partial x} \right. \\
&\quad \left. + i\beta \frac{\partial^2 \rho}{\partial x^2} \right] \\
&= e^{-i\phi} \left[\beta \rho \frac{\partial^2 \varphi}{\partial x^2} + 2\beta \frac{\partial \varphi}{\partial x} \frac{\partial \rho}{\partial x} - \rho \left(\frac{\partial \varphi}{\partial x} \right)^2 + \frac{\partial^2 \rho}{\partial x^2} - i\rho \frac{\partial^2 \varphi}{\partial x^2} - 2i \frac{\partial \varphi}{\partial x} \frac{\partial \rho}{\partial x} - i\beta \rho \left(\frac{\partial \varphi}{\partial x} \right)^2 \right. \\
&\quad \left. + i\beta \frac{\partial^2 \rho}{\partial x^2} \right] \\
&= e^{-i\phi} \left[\beta \rho \frac{\partial^2 \varphi}{\partial x^2} + 2\beta \frac{\partial \varphi}{\partial x} \frac{\partial \rho}{\partial x} - \rho \left(\frac{\partial \varphi}{\partial x} \right)^2 + \frac{\partial^2 \rho}{\partial x^2} - i \left(\rho \frac{\partial^2 \varphi}{\partial x^2} + 2 \frac{\partial \varphi}{\partial x} \frac{\partial \rho}{\partial x} + \beta \rho \left(\frac{\partial \varphi}{\partial x} \right)^2 - \beta \frac{\partial^2 \rho}{\partial x^2} \right) \right]
\end{aligned}$$

I collect all terms from the left- and right-hand sides and obtain

$$\begin{aligned}
&e^{-i\phi} \left[\frac{\partial \rho}{\partial t} - i\rho \cdot \frac{\partial \varphi}{\partial t} \right] \\
&= e^{-i\phi} \left[\beta \rho \frac{\partial^2 \varphi}{\partial x^2} + 2\beta \frac{\partial \varphi}{\partial x} \frac{\partial \rho}{\partial x} - \rho \left(\frac{\partial \varphi}{\partial x} \right)^2 + \frac{\partial^2 \rho}{\partial x^2} - i \left(\rho \frac{\partial^2 \varphi}{\partial x^2} + 2 \frac{\partial \varphi}{\partial x} \frac{\partial \rho}{\partial x} + \beta \rho \left(\frac{\partial \varphi}{\partial x} \right)^2 - \beta \frac{\partial^2 \rho}{\partial x^2} \right) \right]
\end{aligned}$$

Then, I cancel the common factor $e^{-i\phi}$, yielding

$$\begin{aligned}
\frac{\partial \rho}{\partial t} - i\rho \frac{\partial \varphi}{\partial t} &= \beta \rho \frac{\partial^2 \varphi}{\partial x^2} + 2\beta \frac{\partial \varphi}{\partial x} \frac{\partial \rho}{\partial x} - \rho \left(\frac{\partial \varphi}{\partial x} \right)^2 + \frac{\partial^2 \rho}{\partial x^2} - i \left(\rho \frac{\partial^2 \varphi}{\partial x^2} + 2 \frac{\partial \varphi}{\partial x} \frac{\partial \rho}{\partial x} + \beta \rho \left(\frac{\partial \varphi}{\partial x} \right)^2 - \beta \frac{\partial^2 \rho}{\partial x^2} \right)
\end{aligned}$$

Now, I separate the real and imaginary parts and obtain differential equations for the amplitude and phase:

Amplitude:

$$\frac{\partial \rho}{\partial t} = \rho(1 - \rho^2) + \beta \rho \frac{\partial^2 \varphi}{\partial x^2} + 2\beta \frac{\partial \varphi}{\partial x} \frac{\partial \rho}{\partial x} - \rho \left(\frac{\partial \varphi}{\partial x} \right)^2 + \frac{\partial^2 \rho}{\partial x^2} \quad (3.4)$$

Phase:

$$\rho \frac{\partial \varphi}{\partial t} = \rho(\omega + \alpha \rho^2) + \rho \frac{\partial^2 \varphi}{\partial x^2} + 2 \frac{\partial \varphi}{\partial x} \frac{\partial \rho}{\partial x} + \beta \rho \left(\frac{\partial \varphi}{\partial x} \right)^2 - \beta \frac{\partial^2 \rho}{\partial x^2}$$

For $\rho \neq 0$, I get

$$\frac{\partial \varphi}{\partial t} = \omega + \alpha \rho^2 + \frac{\partial^2 \varphi}{\partial x^2} - 2\rho^{-1} \frac{\partial \varphi}{\partial x} \frac{\partial \rho}{\partial x} + \beta \left(\frac{\partial \varphi}{\partial x} \right)^2 - \beta \rho^{-1} \frac{\partial^2 \rho}{\partial x^2} \quad (3.5)$$

After combining the spatial and the non-spatial parts, the amplitude-phase representation (3.4 and 3.5) of the CGLE has been derived. However, these equations are much more complicated than equations (3.2) and (3.3) and are not used for the numerical simulations.

However, the amplitude-phase representation can be used to find easily the basic solution of the CGLE, uniform oscillations described by

$$A_{uo}(t) = \rho_0 e^{-i\Omega t}. \quad (3.6)$$

For uniform oscillations, $|A| = \rho = \rho_0$ is constant in space and time and the phase $\varphi = \Omega t$ is only time-dependent. Inserting this into (3.4) and (3.5), I find that all partial derivatives of ρ are zero, $\frac{\partial \varphi}{\partial t} = \Omega$, all spatial derivatives of φ are zero and

I obtain

$$0 = \rho(1 - \rho^2),$$

$$\Omega = \omega + \alpha \rho^2.$$

The first equation has two solutions $\rho = 0$ and $\rho = 1$, but only a nonzero modulus of the amplitude corresponds to oscillations. The second equation shows how the frequency of oscillations has a constant term and a term that depends in a nonlinear way with the amplitude. Choosing $\rho = 1$, therefore I find

$$\rho_0 = 1,$$

$$\Omega = \omega + \alpha.$$

Therefore, the solution of uniform oscillations can also be written as $A_{uo}(t) = e^{-i(\omega+\alpha)t}$. The stability of this solution is discussed elsewhere (or example, in [9]) and yields the Benjamin-Feir-Newell criterion: uniform oscillations are stable for $1 + \alpha\beta > 0$ and unstable for $1 + \alpha\beta < 0$.

Later, I choose $\omega = 2\pi - \alpha$ and therefore $\Omega = \omega + \alpha = 2\pi - \alpha + \alpha = 2\pi$. Then, the period of uniform oscillations is $T = \frac{2\pi}{\Omega} = 1$ in the time units of the equation.

3.2 Numerical Results

I want to illustrate the main solutions of the complex Ginzburg-Landau equation, obtained by solving Equations (3.2, 3.3) using the explicit Euler method for various initial conditions and for periodic boundary conditions (unless stated otherwise). A 3-point representation is used for the Laplacian. The implementation is made in MATLAB.

Figures 3.1 and 3.2 display the variables (i.e., a and b) against time and space respectively for parameters where uniform oscillations are stable ($1 + \alpha\beta >$

0). The figures were obtained from a simulation with system size 128, total simulation time 5, $\Delta x = 0.32$, $\Delta t = 0.002$, and parameters $\alpha = 1.4$, $\beta = 2$ and $\omega = 2\pi - \alpha$. As initial condition, constant values (in space) for a and b have been chosen: $a = 0.5$ and $b = -0.5$ for all space points. The uniform oscillations in the CGLE are stable and harmonic and Figure 3.1 shows that this is indeed the case. For stable uniform oscillations, all points in space share the same dynamics and since they start from the same initial condition, the temporal curves for different space points are the same. For the same reason, the values of a and b are constant in space, see Figure 3.2.

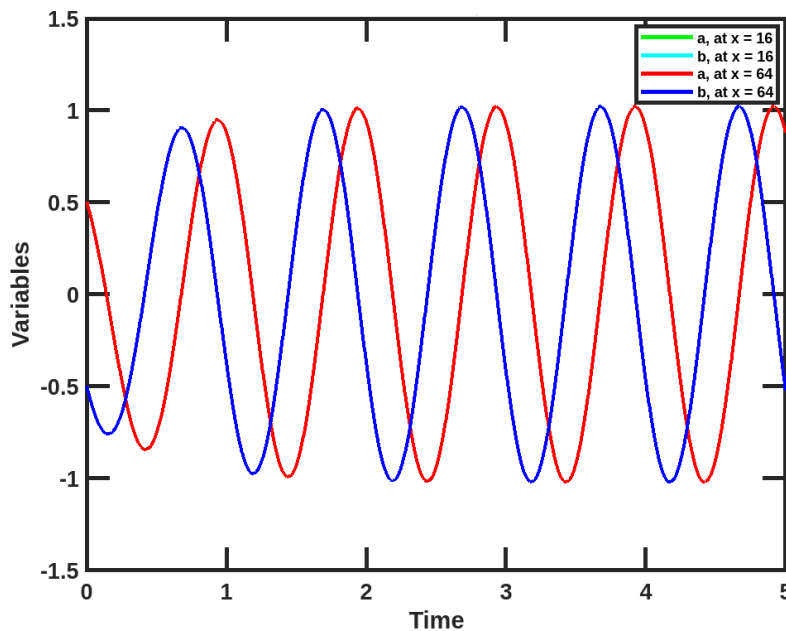


Figure 3.1: The real (a) and imaginary (b) parts of A as a function of time at different space points (see legend).

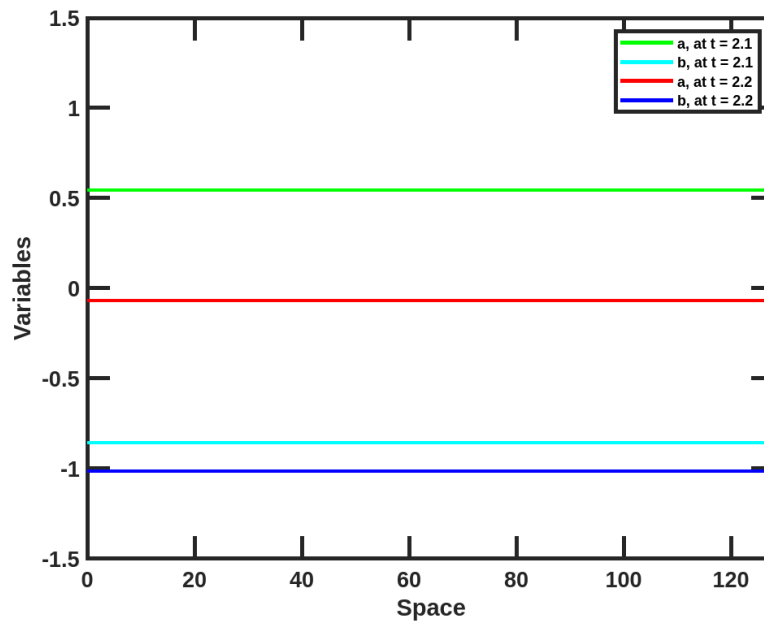


Figure 3.2: The real (a) and imaginary (b) parts of A as a function of space at different time points (see legend).

Figures 3.3 – 3.8 show the results of equations (3.1) and (3.2) when using random initial conditions and a variation of parameters. For each simulation, data at every 50th iteration has been saved to obtain a figure with manageable dimensions. For all these figures, the value of $\omega = 2\pi - \alpha$, whatever α .

Figures 3.3 – 3.8 show uniform oscillations or spatiotemporal chaos (depending on the parameters), where the patterns are shown in greyscale for a and $|A|$. The real part a is well-suited to see waves and the modulus of the amplitude $|A|$ (recall that $|A| = \sqrt{a^2 + b^2}$) tells us if the oscillations have a constant amplitude (as for uniform oscillations) or not (and for chaotic states, the modulus can decrease to zero).

Figures 3.3 – 3.8 are space-time plots, i.e., a and $|A|$ are plotted against time and space where the horizontal axis is space, and the vertical axis is time.

Figures 3.3 and 3.4 are the result of random initial conditions for a and b where positive values of α and β are considered, hence $1 + \alpha\beta > 0$, and stable uniform oscillations are expected to appear. The system size is 128, the simulation time 50 and the numerical parameters are $\Delta x = 0.32$, $\Delta t = 0.002$. Uniform oscillations are indeed found, being represented by periodic changes black-white in time for a as time increases (being spatially uniform) and a constant value of $|A|$ in both space and time. The lighter areas are the higher values of the amplitude, and the darker areas are lower values (close to zero in case of $|A|$). The stable value of $|A|$ is 1, as can be expected for uniform oscillations (see previous section, $\rho_0 = 1$).

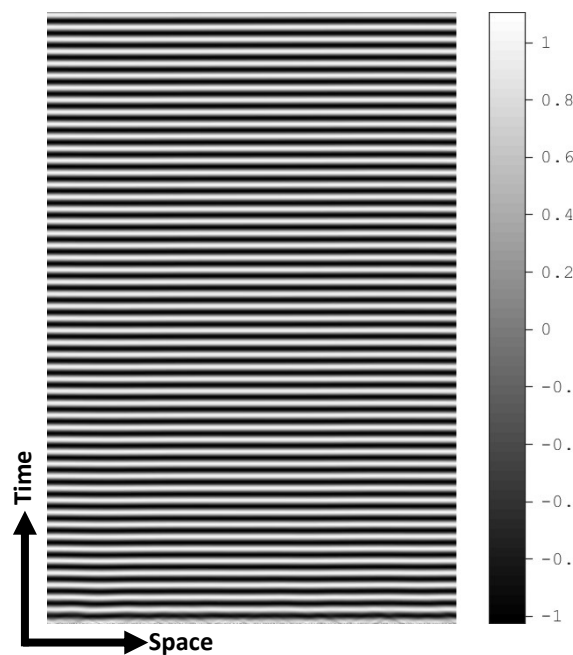


Figure 3.3: Space-time plot of a , showing stable uniform oscillations. Parameters: $\alpha = 1.4$, $\beta = 2$.

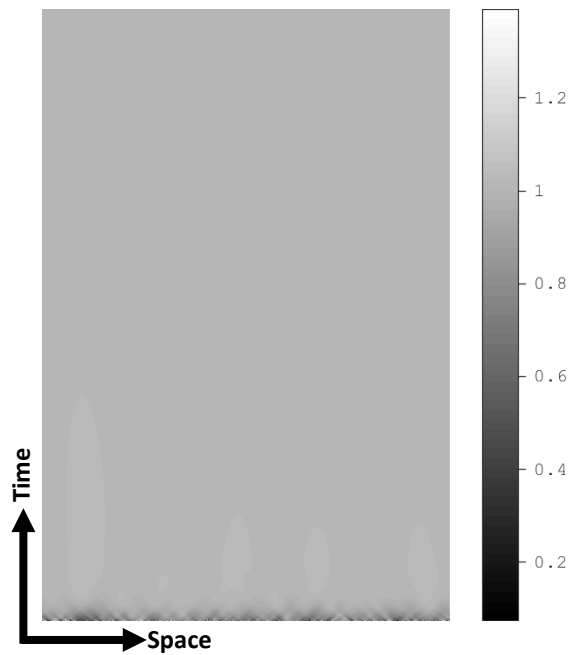


Figure 3.4: Space-time plot of $|A|$, showing that the modulus of oscillations is spatially and temporally constant (and asymptotically approaching 1). Parameters: $\alpha = 1.4$, $\beta = 2$.

Figures 3.5 and 3.6 are the result of random initial conditions for a and b where a sufficiently negative value of α is considered while β is still positive. Since then, the Benjamin-Feir-Newell criterion for instability $1 + \alpha\beta < 0$ is met, it is expected that spatiotemporal chaos appears. The system size is 128, the simulation time 50 and the numerical parameters are $\Delta x = 0.32$, $\Delta t = 0.002$. Indeed, the chaotic state is developing as the number of the time steps increases. Sometimes, the modulus of the amplitude, $|A|$, has values very close to zero. If this is the case, I can talk about *defect* or *amplitude turbulence* [9], if only the phase is chaotic, but the amplitude does not decrease to zero, I can talk about *phase turbulence*. Most of the parameter values used in this thesis correspond to the regime of amplitude turbulence.

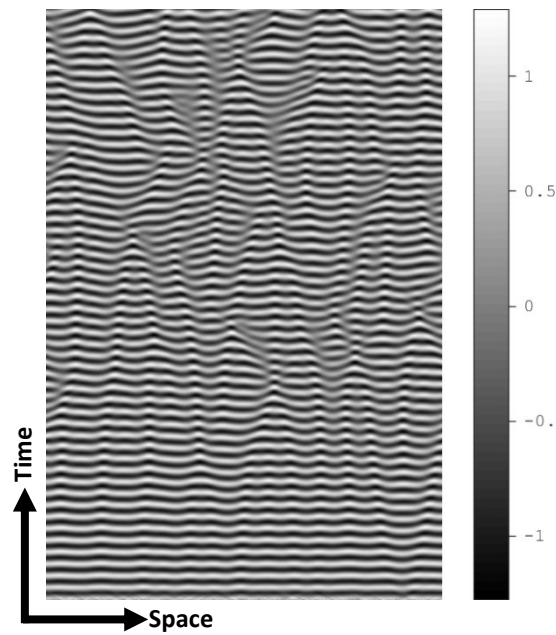


Figure 3.5: Space-time plot of a , showing irregular oscillations (uniform oscillations are unstable). Parameters: $\alpha = -1.4$, $\beta = 2$.

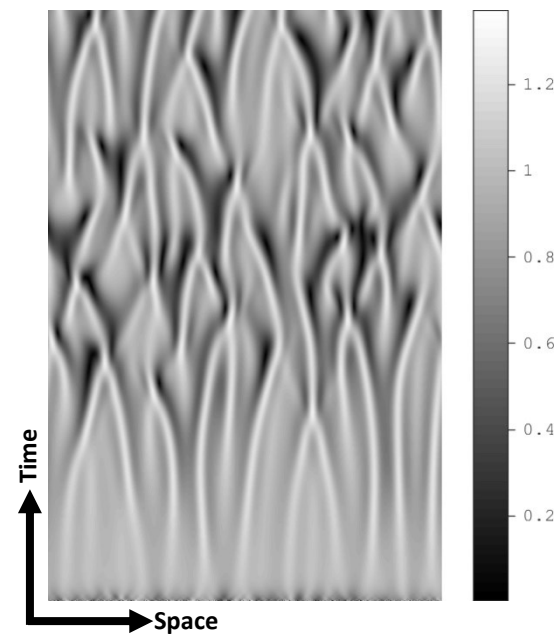


Figure 3.6: Space-time plot of $|A|$, showing that the modulus of oscillations is spatially and temporally irregular (and occasionally approaching zero). Such a pattern is called amplitude turbulence. Parameters: $\alpha = -1.4$, $\beta = 2$.

The following Figures 3.7 and 3.8 is for the same parameters as for Figures 3.5 and 3.6, but the simulation time is not 50 but 100. This simply shows that the spatiotemporal dynamics remains chaotic (amplitude defects keep occurring).

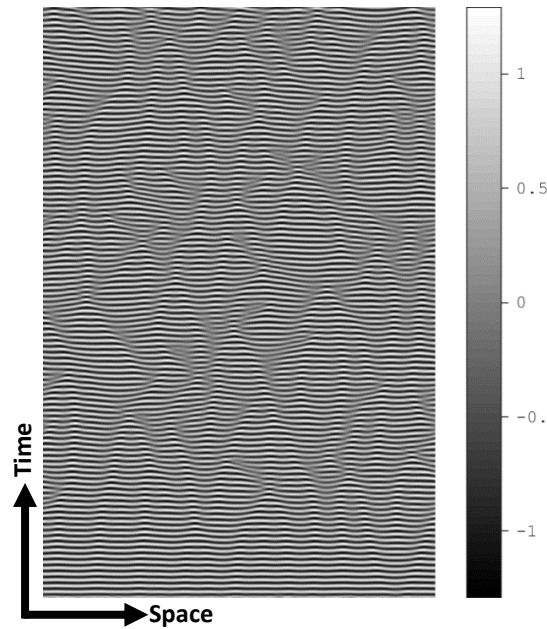


Figure 3.7: Space-time plot of a . Same as Fig. 3.5, but with longer simulation time 100. Parameters: $\alpha = -1.4$, $\beta = 2$.

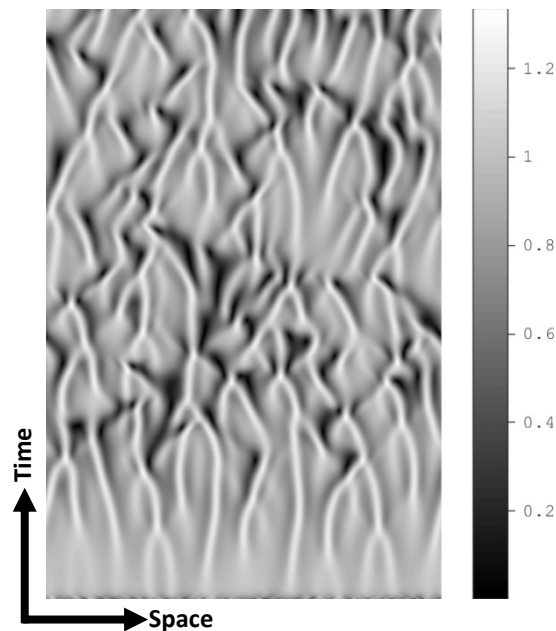


Figure 3.8: Space-time plot of $|A|$. Same as Fig. 3.6, but with longer simulation time 100. Parameters: $\alpha = -1.4$, $\beta = 2$.

Chapter 4

Travelling waves

This chapter discusses the CGLE system with feedback and studies the travelling wave solution.

4.1 The CGLE with feedback and uniform oscillations

Here, I present the CGLE with time-delay feedback with local and global contributions, as introduced first in [13], and mentioned in Chapter 1:

$$\frac{\partial A}{\partial t} = (1 - i\omega)A - (1 + i\alpha)|A|^2A + (1 + i\beta)\frac{\partial^2 A}{\partial x^2} + F \quad (4.1)$$

where A = complex oscillation amplitude

ω = linear frequency parameter

α = nonlinear frequency parameter

β = linear dispersion coefficient

F = feedback term

$$F = \mu \cdot e^{i\xi} \cdot [m_l\{A(x, t - \tau) - A(x, t)\} + m_g\{\bar{A}(t - \tau) - \bar{A}(t)\}], \quad (4.2)$$

where μ = feedback strength

ξ = phase shift

τ = delay time

m_g = global feedback strength

m_l = local feedback strength

and $\bar{A}(t) = \frac{1}{L} \int_0^L A(x, t) dx$

where, \bar{A} = spatial average

L = one-dimensional system length

I now give the formulations in real and imaginary parts for the numerical implementation.

Now replacing A with $(a + ib)$ in both sides of the CGLE with feedback (4.1, 4.2), similar to the treatment in Chapter 3, the equations for real and imaginary parts have been obtained, (see Appendix):

Real Part:

$$\begin{aligned} \frac{\partial a}{\partial t} = & a\{1 - (a^2 + b^2)\} + b\{\omega + \alpha(a^2 + b^2)\} + \frac{\partial^2}{\partial x^2}(a - \beta b) \\ & + \mu \cdot \cos \xi \cdot [m_l \cdot \{a(x, t - \tau) - a(x, t)\} + m_g \cdot \{\bar{a}(x, t - \tau) - \bar{a}(x, t)\}] \\ - \mu \cdot \sin \xi \cdot & [m_l \cdot \{b(x, t - \tau) - b(x, t)\} + m_g \cdot \{\bar{b}(x, t - \tau) - \bar{b}(x, t)\}] \end{aligned} \quad (4.3a)$$

Imaginary Part:

$$\begin{aligned} \frac{\partial b}{\partial t} = & b\{1 - (a^2 + b^2)\} - a\{\omega + \alpha(a^2 + b^2)\} + \frac{\partial^2}{\partial x^2}(\beta a + b) \\ & + \mu \cdot \cos \xi \cdot [m_l \cdot \{b(x, t - \tau) - b(x, t)\} + m_g \cdot \{\bar{b}(x, t - \tau) - \bar{b}(x, t)\}] \\ + \mu \cdot \sin \xi \cdot & [m_l \cdot \{a(x, t - \tau) - a(x, t)\} + m_g \cdot \{\bar{a}(x, t - \tau) - \bar{a}(x, t)\}] \end{aligned} \quad (4.3b)$$

These equations have been implemented in MATLAB to generate the numerical results, using again the Euler method and a 3-point representation of the Laplacian.

4.2 From uniform oscillations to travelling waves

Before studying travelling waves in more detail, it is useful to consider the simpler plane waves, which can be seen are a special type of travelling waves, namely those with a constant amplitude. At any given point of space x and time t , plane waves can be described as:

$$A(x, t) = \rho e^{-i(\Omega t - kx)},$$

where $\rho = |A|$ is the modulus of the amplitude A ; k is the *wavenumber* $= \frac{2\pi}{\lambda}$, and Ω is the *angular velocity* of the waves with *wavenumber* k .

Another interesting solution are standing waves. They have been first reported for this model in [13], then interpreted as an instability of uniform oscillations in [18], and later investigated in detail in [19]. The main results can be described as follows: Standing waves can be found in parameter areas which are adjacent to regions where stable uniform oscillations have been. The amplitude profile of standing waves does not move in space, it is always constant with respect to time. At any given point of space (x) and time (t), standing waves can be described as:

$$A(x, t) = \rho(x) e^{-i(\Omega t - kx)},$$

where $\rho(x)$ is now a space-dependent (real) amplitude (rest as above).

In numerical research published in 2007 [13], travelling waves have been reported, where now the real amplitude depends on both time and space:

$$A(x, t) = \rho(x, t)e^{-i(\Omega t - kx)}.$$

However, such patterns were just reported in simulations, but not discussed in more detail. Before considering more simulations on these, the different patterns mentioned can be compared in Table 4.1.

Table 4.1 Different wave patterns

Pattern	ρ time dependent	ρ space dependent	General Equation
Travelling wave	Yes	Yes	$A(x, t) = \rho(x, t)e^{-i(\Omega t - kx)}$
Standing wave	No	Yes	$A(x, t) = \rho(x)e^{-i(\Omega t - kx)}$
Plane wave	No	No	$A(x, t) = \rho e^{-i(\Omega t - kx)}$
Uniform oscillation	No	No	$A(t) = \rho e^{-i\Omega t}$

In Figure 4.1, a qualitative sketch distinguishes in space-time diagrams these four patterns: uniform oscillations, plane waves, standing waves and travelling waves.

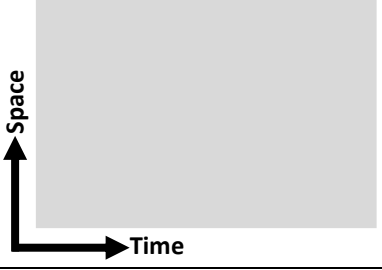
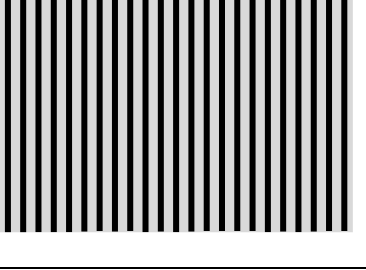
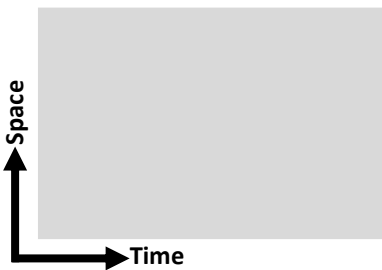
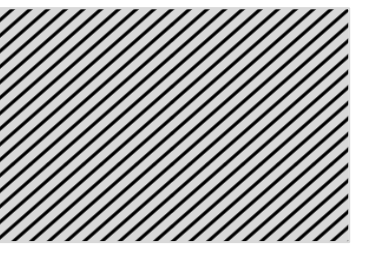
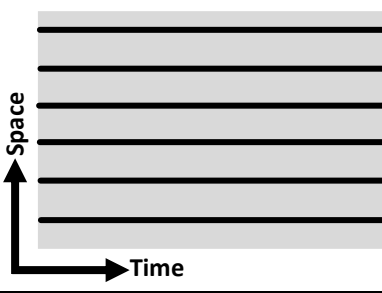
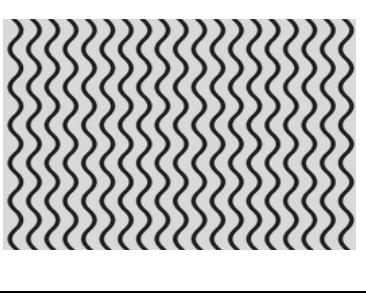
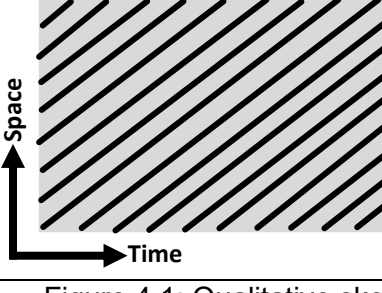
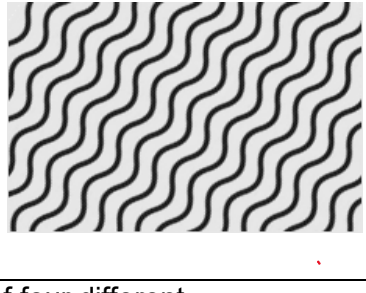
Type of Wave	$ A $	$Re A$
Uniform Oscillation		
Plane Waves		
Standing Waves		
Travelling Waves		

Figure 4.1: Qualitative sketch of four different wave patterns as seen in space-time plots.

Since Figure 4.1 is just a qualitative sketch, in Figure 4.2, I present actual space-time plots as reported in different publications.

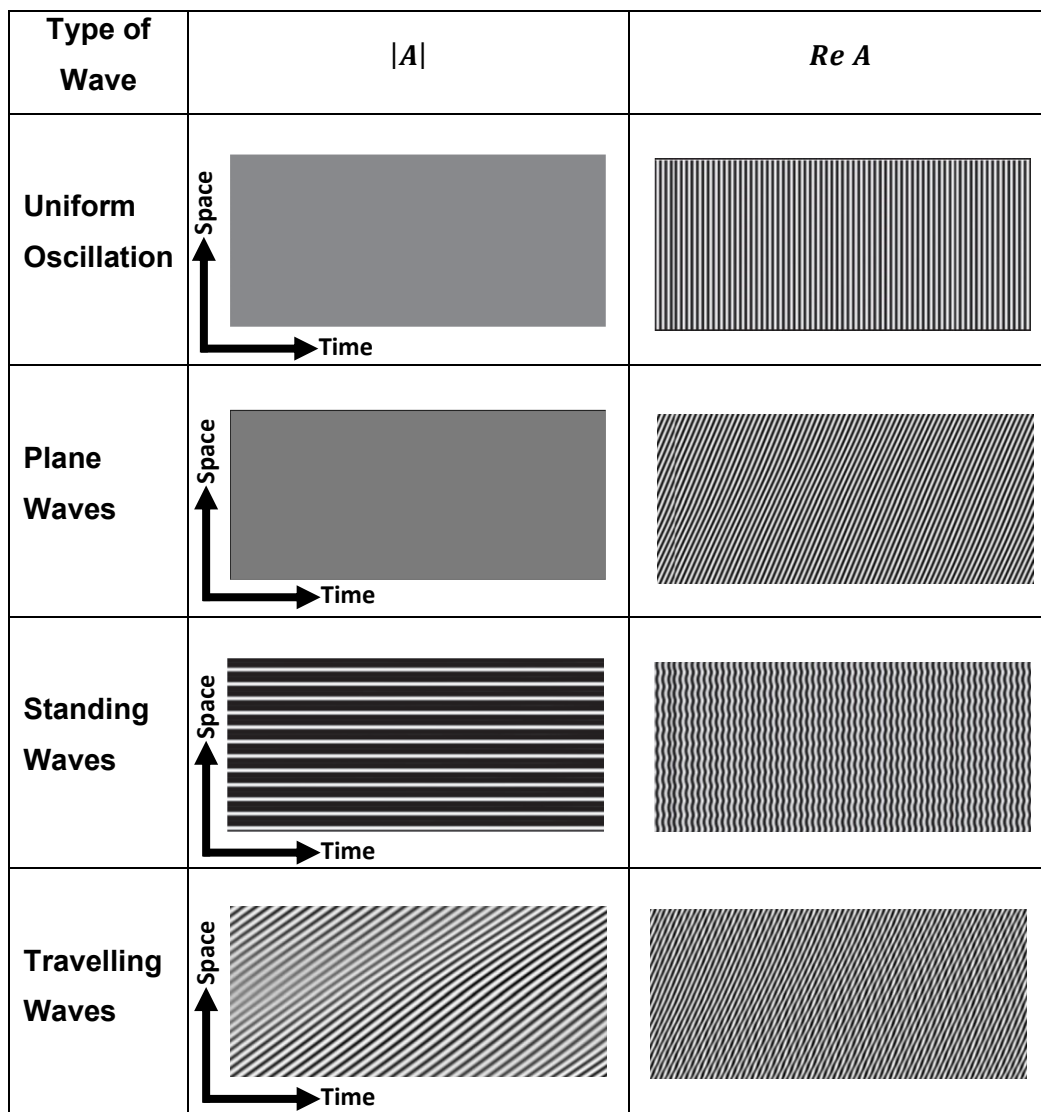


Figure 4.2: Uniform oscillations, plane waves, standing waves and travelling waves as reported earlier. Parameters and numerical parameters are found in the original publications, i.e., in [13] for plane and travelling waves and [18] for uniform oscillations and standing waves.

4.3 Simulations of transient travelling waves

Since in none of the previous publications, travelling waves were discussed, here, I investigate travelling waves in this model. Motivated by the results published in [13], simulations were done for a constant feedback strength

$\mu = 0.6$ and time delay $\tau = 1.1$ varying the initial wavenumber. The global and local parameter were set to 0.2 and 0.8, respectively. The value of α set to -1.4 and β is 2; $\Delta x = 0.32$ and $\Delta t = 0.002$; system size 128.

To set the initial condition, the number of initial waves filling the system was chosen, which is n in this case, such that an integer number of waves $n\lambda$ is filling the system of length L . It has been chosen all integer values for n from 1 to 20 and therefore preparing initial conditions with wavenumber $2\pi \frac{n}{L}$.

Then, short (up to 1000 iterations, which corresponds to a time interval $T = 100$) and long (up to 10000 iterations, which corresponds to a time interval $T = 1000$) simulations have been performed on each initial wavenumber.

In the simulations performed here, such travelling waves were asymptotically unstable, but their transient existence for up to tens of passages through the system (with periodic boundary conditions) for some of the initial conditions make them an interesting pattern to study. Some of these waves are relatively harmonic and others non-harmonic.

Figure 4.4 shows simulations where the initial condition led successfully into a travelling wave state, but which was later found to be a transient.

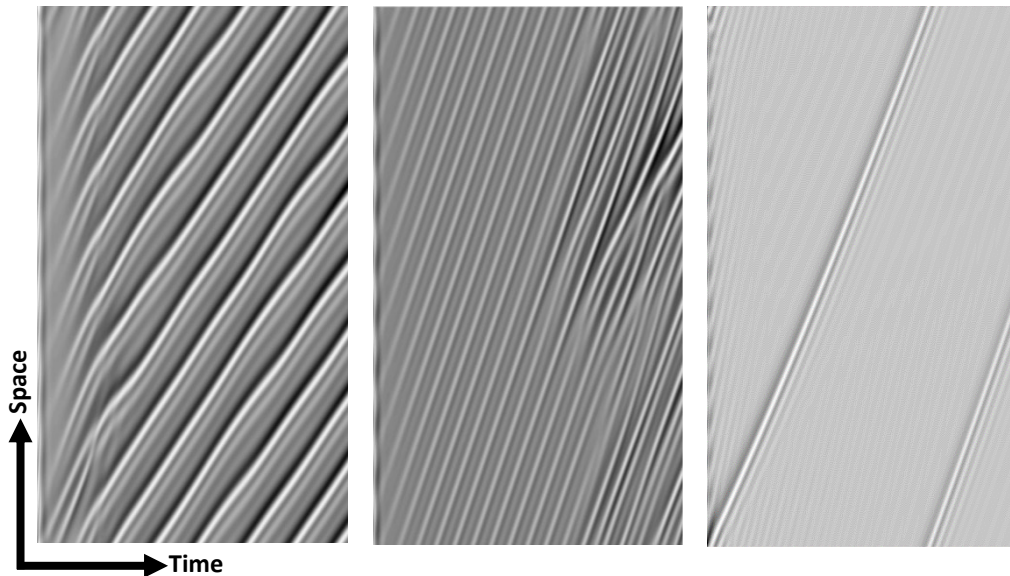


Figure 4.3: Short simulations (time interval $T = 100$) for transient travelling waves with initial wavenumbers corresponding to 8, 10, and 15 waves filling the system. The shown variable is $|A|$.

As initial condition, I have created a travelling wave train with $n = 8$ waves, corresponding to a travelling wave with wavenumber 0.393 (Figure 4.4, left). During the transient, a wave train with 8 waves developed, however it decayed later. The travelling wave has a nonmonotonic tail as can be seen by the change of light to dark grey in the back of the main wave.

In a different simulation, with an initial condition composed of $n = 10$, corresponding to an initial wavenumber 0.491 (Figure 4.4, centre), also a transient travelling waves has been found, in this case developing quickly in an irregular state of merging wave fronts and then to uniform oscillations.

Finally, for an initial wavenumber 0.736, corresponding to a wave train of $n = 15$ waves (Figure 4.4, right) also a travelling wave has been found. However, it resembles more a solitary wave than a travelling wave since the wavelength is equal the system size, hence having 1 wave. This wave later decays to uniform oscillations, too.

In longer simulations of the same initial wavenumbers, none of these kept the same pattern, and gave rise to uniform oscillations, as can be seen by the figures for $|A|$, where a spatially and temporally constant value is obtained, see Figure 4.5.

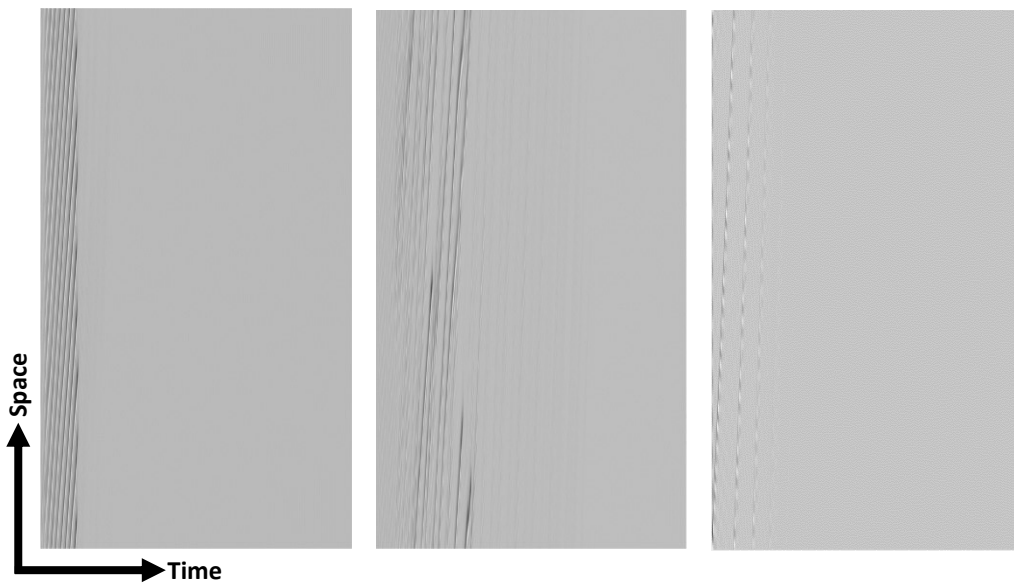


Figure 4.4: Long simulations (time interval $T = 1000$). For rest of parameters, see Figure 4.4.

Figure 4.5 shows the short simulation ($T = 50$) where the variables (i.e. Real A and $|A|$) data were taken for the time moment at 500. As it has been seen in Figure 4.4, at higher wave numbers the variables fluctuation gets more smoother, which indicates waves are decaying to uniform oscillation.

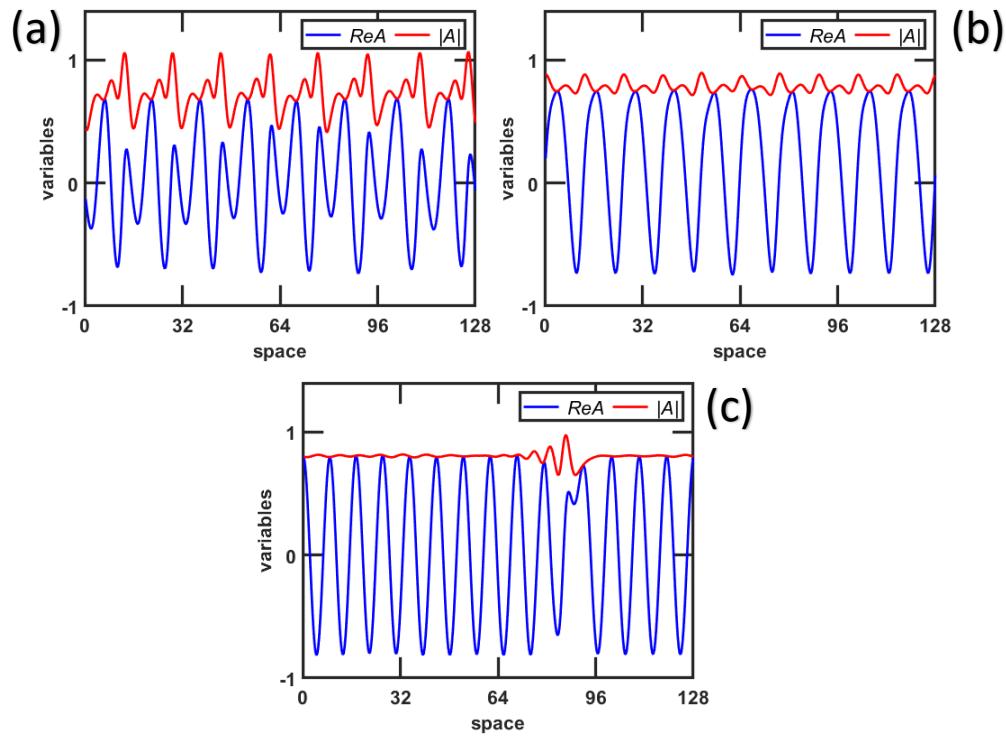


Figure 4.5: Short simulations (time interval $T = 50$). At time moment 500 for $n = 8$ waves (a), $n = 10$ waves (b), $n = 15$ waves (c). For rest of parameters, see Figure 4.4.

Chapter 5

Spot patterns

In this chapter, I investigate *spot patterns* (defined on page 55). Since no spot patterns have been observed in the model studied in Chapter 4, I introduce a modification into the equation. After presenting this model, I discuss the numerical evidence for spot patterns, their stability, and multiple spot patterns.

5.1 Model for local feedback

Here, I introduce the CGLE for a one-dimensional medium with a local time-delayed feedback F defined by

$$\frac{\partial A}{\partial t} = (1 - i\omega)A - (1 + i\alpha)|A|^2A + (1 + i\beta)\frac{\partial^2 A}{\partial x^2} + F \quad (5.1)$$

where A = complex oscillation amplitude

ω = linear frequency parameter

α = nonlinear frequency parameter

β = linear dispersion coefficient

F = feedback term

$$F = \mu \cdot e^{i\xi} \cdot \{A(x_0, t - \tau) - A(x, t)\}, \quad (5.2)$$

where μ = feedback strength

ξ = phase shift

τ = delay time

x_0 = feedback point, a single gridpoint of the discretized medium of length L

The feedback is a space-dependent function in two ways: first, due to the dependence on A and second due to the dependence on x_0 which assigns a special importance to the dynamics at this point. The strength of the feedback is proportional to the difference of the current state and a delayed state, as in Chapter 4. This model is similar to the model used in Chapter 4 but has no global contribution and has this special feedback point x_0 .

It can be noted that the solution of feedback-induced uniform oscillations is given by

$$A(t) = \rho e^{-i\Omega t},$$

with
$$\rho^2 = 1 + \mu(\cos(\xi + \Omega\tau) - \cos \xi)$$

and
$$\Omega = \omega + \alpha + \mu(\alpha(\cos(\xi + \Omega\tau) - \cos \xi) - (\sin(\xi + \Omega\tau) - \sin \xi)),$$

where the solution for Ω must be found numerically using root-finding methods since Ω appears on both sides of the equation. This is essentially the same solution as for the model in Chapter 4, the only difference being that instead of μ , there we have $\mu(m_l + m_g)$.

5.2 Numerical study of spot patterns

I have performed extensive spatiotemporal simulations of equations (5.1, 5.2) for a one-dimensional system with size $L = 128$ and spatial resolution $\Delta x = 0.32$ (400 grid points). For time integration, I use an explicit Euler scheme with $\Delta t = 0.002$. The Laplacian operator is discretized using a next-neighbour representation. I apply periodic boundary conditions and the initial conditions (unless stated otherwise) consist of developed spatiotemporal chaos. Due to the periodic boundary condition, the medium is uniform if $\mu = 0$ (and hence $F = 0$). However, if $\mu \neq 0$, the dependence of F on x_0 breaks this symmetry and without loss of generality (and unless stated otherwise) I set $x_0 = 0$ for $\mu \neq 0$. The feedback refers to one grid point only. Throughout this chapter, the CGLE parameters are kept constant: the nonlinear frequency parameter $\alpha = -1.4$, the linear dispersion coefficient $\beta = 2$, and the linear frequency parameter $\omega = 2\pi - \alpha$. For all but a few simulations (and then stated), the phase shift between the feedback and the dynamics is chosen to be $\xi = \frac{\pi}{2}$.

The main patterns are the same as for the model discussed in Chapter 4, in particular uniform oscillations, standing waves and spatiotemporal chaos, for an overview see Figure 5.1. However, a novel pattern has been observed in the simulations and that is displayed in Figure 5.2 where it shows space-time plots and a spatial profile in its asymptotic (and therefore stable) regime.

The wave pattern is characterized by uniform oscillations that are perturbed in a localized spatial region. The space-time plot for ReA (Figure 5.2(a)) demonstrates that the oscillation frequency is the same throughout the medium

and the main difference between the oscillations inside the region and outside is their *phase* and *amplitude*. For the specific parameters of the simulation, the localized oscillation advances the background oscillation approximately one third of the period. The (modulus of the) *amplitude* changes strongly in a small area of the medium (Figure 5.2(b,c)) and decreases to approximately 40% of the amplitude of the background. Therefore, this pattern referred as **spot pattern**. However, it is important to note that the centre of the spot (around $x = 9.4$) does not coincide with the location of the feedback point ($x_0 = 0$).

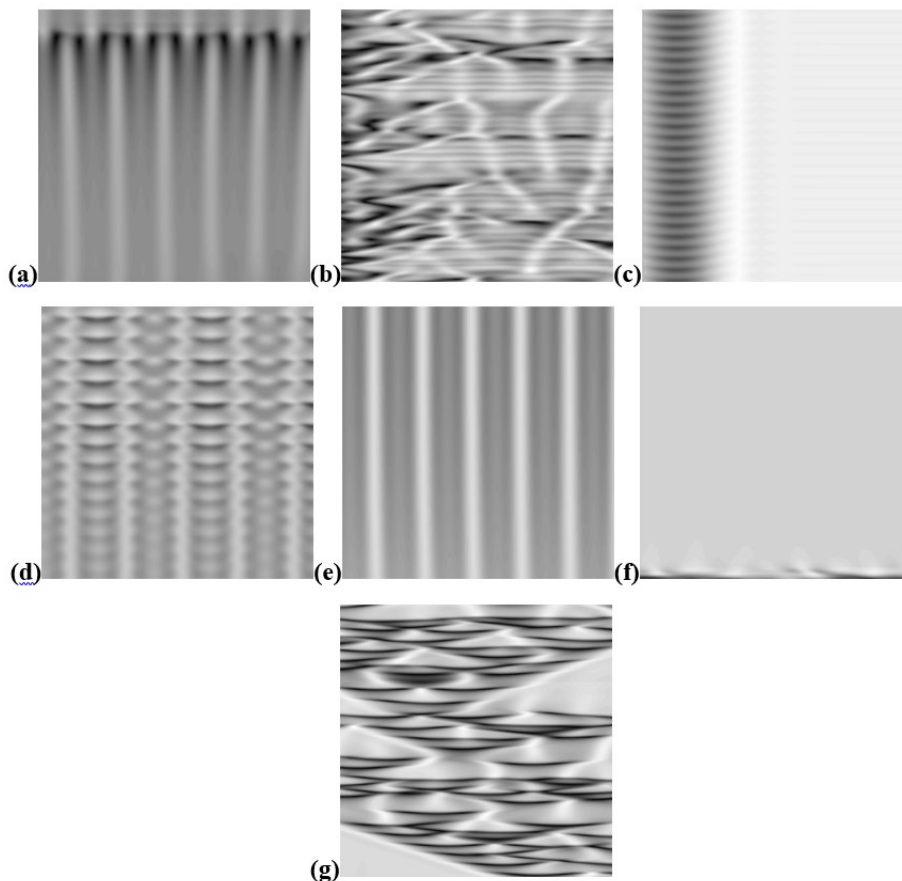


Figure 5.1: Space-time diagrams for $|A|$ in grey scale - (a) unstable standing wave, (b) spatiotemporal chaos, (c) cluster, (d) breathing and unstable standing wave, (e) stable standing wave, (f) uniform oscillation, and (g) spatiotemporal chaos. Space is horizontal, time is vertical axis moving upwards.

The pattern has an intrinsic localized character. As such, in a sufficiently large system more than one spots may be stabilized, as shown in Figure 5.3(a,b). There, after an initial transient (not shown here), the medium displays two spots, one centred around $x=9$, the other one at $x=51$. Both spots have the same amplitude profile. I come back to multiple spot solutions below.

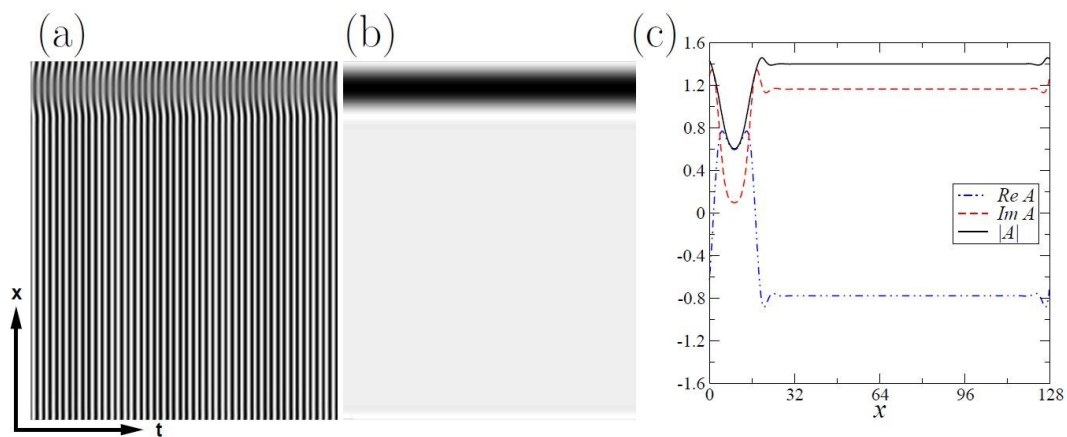


Figure 5.2: Spot solution. (a) Space-time plots of a spot solution in the asymptotic regime for ReA (a) and $|A|$ (b). (c) Spatial profiles for ReA , ImA , and $|A|$. The feedback parameters are: $\mu=0.9$, $\tau=0.8$, $\xi = \frac{\pi}{2}$, $x_0 = 0$. The displayed time interval is $t = 50$ (a,b). The center of the spot pattern is approximately located at $x = 9.4$. In the space-time plots, black (white) refers to the minimum (maximum) values in the interval. In (a), the values of ReA are between -1.46 and +1.46 and in (b) the values of $|A|$ are between 0.60 and 1.46.

The time-delayed feedback is also able to induce transient cascades of spot patterns, as displayed in Figure 5.3(c,d). Besides the dependence on system parameters, the asymptotic state of such cascades depends very sensitively on the initial condition and is either a persisting chaotic state, uniform oscillations, or a spot pattern (with one or multiple spots).

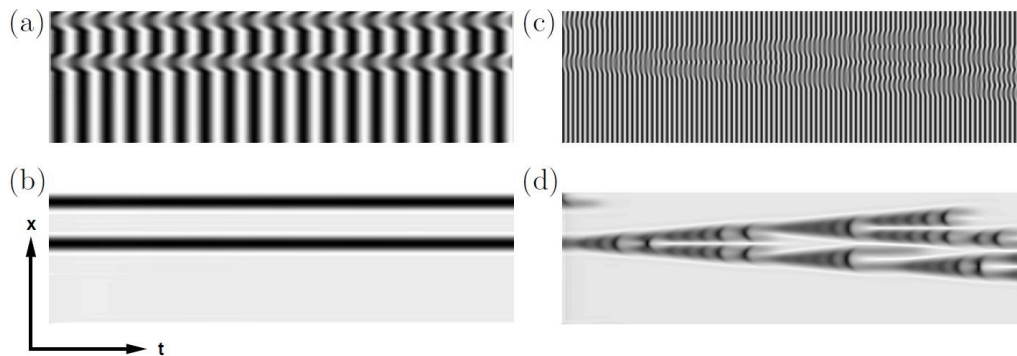


Figure 5.3: Spot solutions. (a,b) Space-time plots for two spot solutions in the asymptotic regime for ReA (a) and $|A|$ (b). The displayed time interval is $T = 20$. Other parameters are as given in Figure 5.2. (c,d) Space-time plots for a transient cascade of spots for ReA (c) and $|A|$ (d). The parameters are the same as in (a), but the initial state has been perturbed in the upper spot, leading to a destabilization of the overall pattern. The displayed time interval is $T = 100$.

In this example, the cascades have been introduced by perturbing a stable two-spot state (of (a,b)) by changing ReA strongly in one spot. The fact that this perturbation leads to a destabilization of the other spot shows that the spot pattern is not robust with respect to large perturbations. Since at every different location x , the feedback contains a term corresponding to the value of $A(x_0, t - \tau)$, the local dynamics depends on both the local previous state and the time-delayed state at x_0 .

While cascade-like patterns have been observed in various simulations where large perturbations or parameter changes have been applied to a stable spot pattern, it is more interesting to see the generic behaviour of spot patterns when the perturbations are small or when parameters are changed in small steps. This is investigated in the next section.

5.3 Stability of spot patterns

The application of small parameter changes to a stable spot pattern usually does not lead to its disappearance, but to a new spot pattern that has adjusted its oscillation frequency, amplitude, and extension to the new parameters. The spot pattern is therefore robust.

However, spot solutions can eventually become unstable once a critical parameter value is reached. Now, three main types of destabilizations of the spot pattern have been found: first, the spot becomes smaller and eventually its size shrinks to zero: that named as a disappearing spot. Second, the spot becomes larger and merges into the background uniform oscillations: that named as an exploding spot. Third, the spot size starts to oscillate with a soft onset, i.e., with small oscillation amplitude, an instability denoted as breathing spots. Not only the spot size oscillates, but also the amplitude values within the spot. These three types are illustrated in Figure 5.4 via space-time plots for $|A|$.

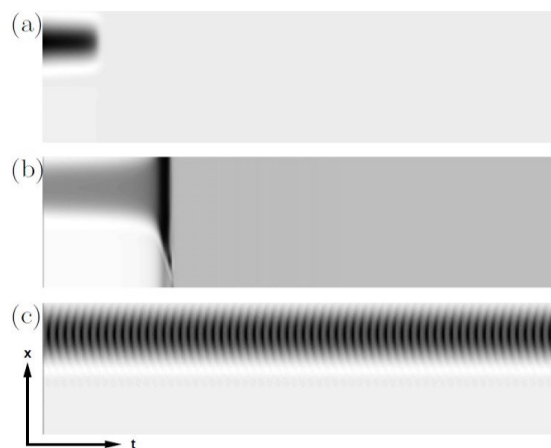


Figure 5.4: Destabilization of spot solutions. Displayed are space-time plots for $|A|$ (time interval $T = 50$) in the transient (a,b) and asymptotic (c) regime. (a) Disappearing spot for $\mu = 0.972$ and $\tau = 0.8$. (b) Exploding spot for $\mu = 1.8$ and $\tau = 1.044$. (c) Breathing spot for $\mu = 0.824$ and $\tau = 0.8$. Other parameters are as given in Figure 5.2.

In order to understand where the spot patterns are observed in parameter space, I have performed systematic simulations: I started from a stable spot pattern and changed the μ or τ value in small steps and waited until the resulting pattern had stabilized, before changing the value again. At some critical value of μ or τ , the spot pattern becomes unstable, marking the boundary of the stability region.

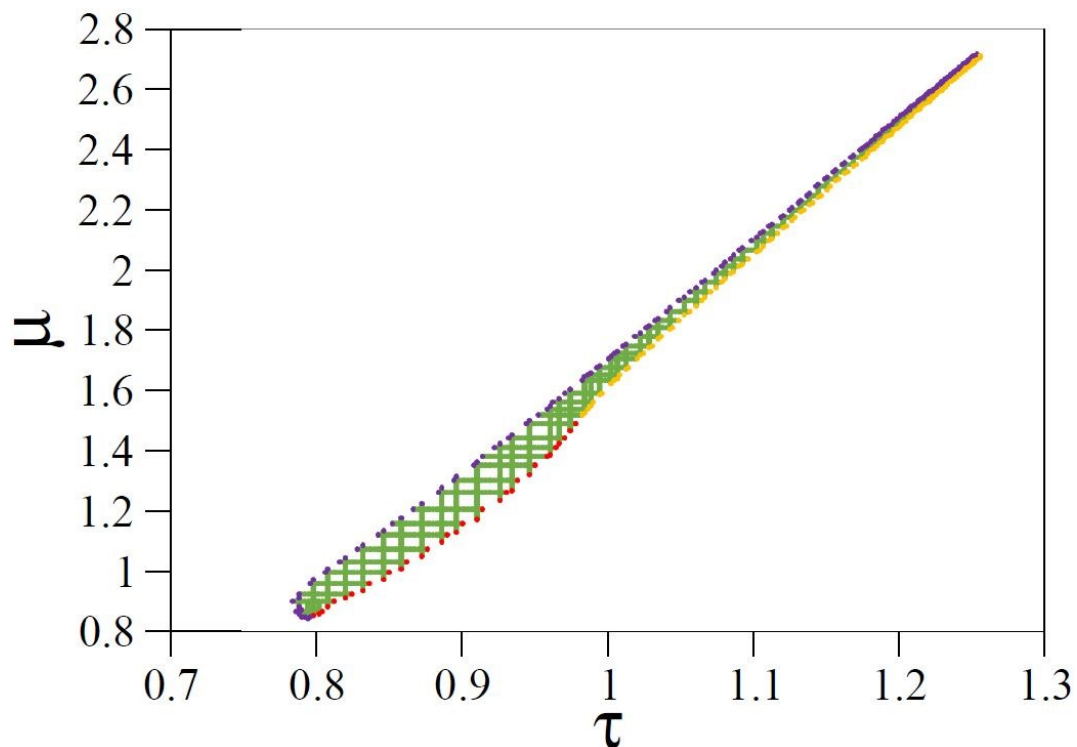


Figure 5.5: Stability region for the spot solution in parameter space spanned by μ and τ . Green dots show simulations with an asymptotic stable spot solution, red dots correspond to simulations where spot solutions started to oscillate in size (lower boundary for $\tau < 1$), yellow dots to simulations where the spot size increased until the spot disappeared (lower boundary for $\tau > 1$) and violet dots to simulations where the spot disappeared via shrinking (upper boundary). Step size in μ is 0.005 and in τ is 0.002 and simulation time is up to 200 to determine stability. The parameter τ has only been changed in decreasing order, ensuring that always $\tau/\Delta t$ meaningful data points were available in the initial condition of the subsequent simulation. Other parameters are as given in Figure 5.2.

The resulting stability region is shown in Figure 5.5. The area seems quite thin, however, the displayed ranges of both τ and μ are actually quite large. Also, the area extends to relatively high feedback strengths, especially in comparison to previously reported stability areas for a similar model [13, 18, 19].

In the interior of the stability area, single spots of varying size (see below) are found. The boundary of the area is limited by three different instabilities. The simplest one is if for a stable spot (at constant τ), the feedback strength μ is increased. Then, the spot size decreases and, at the boundary of the stability area, eventually shrinks to zero (violet dots in Figure 5.5). If the delay time is larger than $\tau \approx 1$ and if the feedback strength μ is decreased, the spot size increases but remains a stable spot with a stable asymptotic extension until, at the boundary of the stability area, the spot merges with the background oscillations (yellow dots in Figure 5.5). If the delay time is smaller than $\tau \approx 1$ and if the feedback strength μ is decreased, the spot size and amplitude values in the spot start to oscillate (red dots in Figure 5.5). The stability area has been defined as the value of μ at which the oscillations become self-sustained, i.e., are not damped.

The spatial extension of the spot solution is determined by the system parameters. This is shown in Figure 5.6. I characterize the spatial extension through the half-maximum width S as determined by $|A|$ (after subtraction of the background value of $|A|$). To simplify the procedure and since it was mainly interested to show that the spot size indeed changes as a function of parameters, no interpolation has been performed between grid points to obtain a precise value of S (nevertheless, the spot extension is always larger than the mesh size Δx).

In Figure 5.6(a), S is shown as function of μ for $\tau = 0.8$ for the range of stable spot patterns. As the feedback strength increases, the size becomes smaller and as a critical μ value is passed, the spot rapidly shrinks and disappears. For low feedback strengths, the spot becomes unstable with respect to oscillations of the size.

In Figure 5.6(b), S is shown as function of τ for $\mu = 0.9$ for the range of stable spot patterns. In this case, the oscillations in size are observed as the delay time is increased, while the size quickly shrinks to zero for decreasing delay times. Finally, the figure 5.6(c) shows that the size S can also be varied by changes of the parameter ξ .

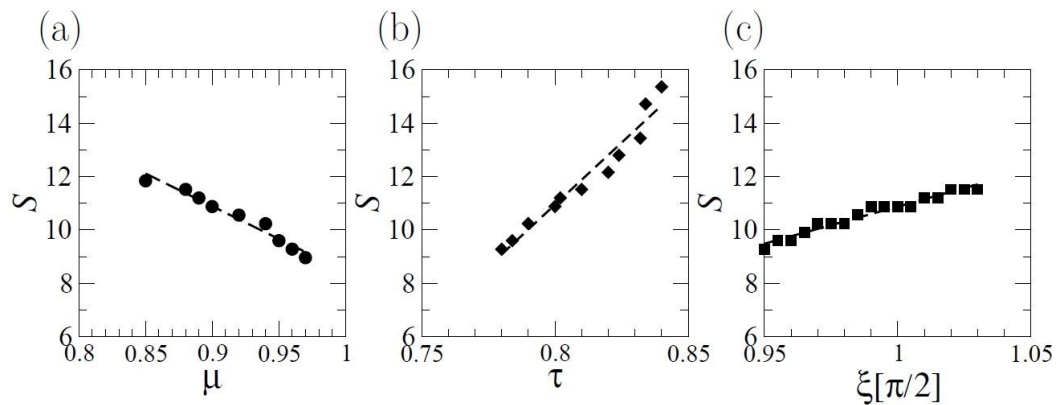


Figure 5.6: Spatial size S of a single stable spot solution. (a) $S(\mu)$ for $\tau = 0.8$ and $\xi = \pi/2$. (b) $S(\tau)$ for $\mu = 0.9$ and $\xi = \pi/2$. (c) $S(\xi)$ for $\tau = 0.8$ and $\mu = 0.9$. The dashed lines are linear regression curves only meant as an aid to the eye. Other parameters are as given in Figure 5.2.

5.4 Multiple spot patterns

The system is uniform, with the only exception being the feedback term that depends on x_0 . Therefore, it is of interest to study how a stable spot pattern reacts to a change of x_0 . I recall that until now, $x_0 = 0$, i.e., it has been seen that the feedback point is located near the boundary of the spot solution, which itself is centred at $x = 9.4$ (see Figure 5.2).

Obviously, in a system with periodic boundary conditions, there is nothing special about selecting $x_0 = 0$. To remove that apparently special choice and confirm the self-organized nature of the pattern, it was chosen to select $x_0 = 12.8$ (grid point 40) and shift all data points (including the time-delayed values) of ReA and ImA for a stable spot pattern by the same number of grid points. The result, not shown here, and completely consistent with the expectations, is a stable spot pattern whose centre is now located at $x = 12.8 + 9.4 = 22.2$ (grid point 70).

I was interested to find out what influence is exerted by the specific location x_0 on a stable spot pattern and how sensitive the pattern reacts to changes of the feedback point. To this end, I use the stable spot pattern at $x_0 = 12.8$ (grid point 40) as initial condition for a systematic change of x_0 without shifting the data sets simultaneously. Of course, this is equivalent to shifting the pattern (including the time-delayed values) by the same amount in the opposite direction maintaining x_0 fixed.

The results in Figure 5.7 show the asymptotic state (found after simulation times of up to $t = 800$) once x_0 has moved from grid point 40 to a new position (for convenience, where it specifies a spatial position, including x_0 , via its grid point).

The first observation is that small changes of x_0 do not lead to a change of the pattern. For example, if $x_0 \in [39,42]$, and therefore not only at $x_0 = 40$, the stable spot solution has been observed. The second observation is that the stable spot solution is maintained at the same position without any notable change if $x_0 \in [99,102]$. This has a simple explanation: The centre of a stable spot pattern (approximately at grid point 70) does not coincide with the feedback point, but, as it has been seen above (Figure 5.2(c)), the feedback point is located near the boundary of the pattern. Since a spot pattern in one space dimension has two symmetrical boundaries (visible in the profile of $|A|$), the feedback point can be located near either boundary.

This symmetry generalizes to breathing patterns: If $x_0 \in [35,38]$, the observed pattern is a single spot, however, with breathing dynamics. Specifically, for $x_0 = 38$, the breathing is relatively smooth, while its amplitude becomes larger for decreasing x_0 and at $x_0 = 35$ it displays a strong breathing dynamics. At $x_0 = 34$, breathing has observed only as a transient before the spot disappears and the asymptotic state of uniform oscillations is reached. For $x_0 \in [103,105]$ breathing spots with increasing amplitude and for $x_0 = 106$ the asymptotic state consists of uniform oscillations have been observed.

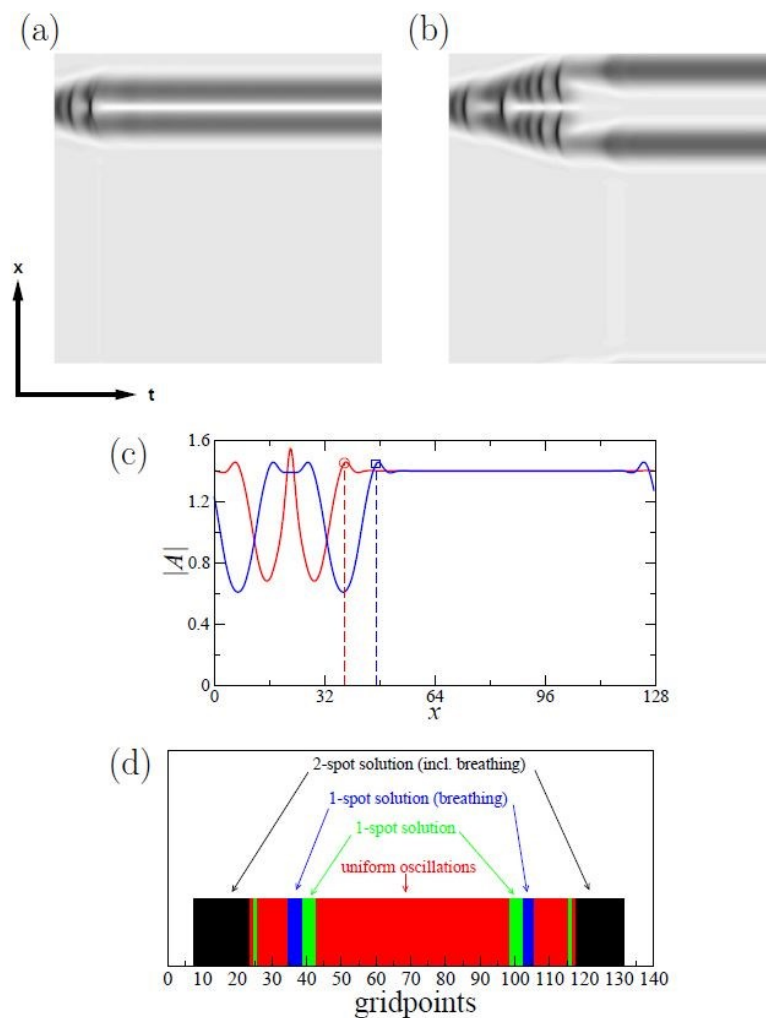


Figure 5.7: Two spots for $\tau = 0.8$ and $\mu = 0.9$ after switching from $x_0 = 40$ to (a) $x_0 = 118$, (b) $x_0 = 147$ (positions given in grid points). The straight solid lines indicate the positions of x_0 . Other parameters are as given in Figure 5.2. (c) Spatial profile of $|A|$ for the solutions from (a) in red and (b) in blue. The x_0 positions are indicated with a red circle and dashed drop line (grid point 118 corresponds to $x \approx 37.8$ for the simulation in (a)) and with a blue square and dashed drop line (grid point 147 corresponds to $x \approx 47$ for the simulation in (b)), respectively. $|A(x_0) \approx 1.45|$ in both cases. Other parameters are as given in Figure 5.2. (d) Main solutions found after switching from $x_0 = 40$ to the gridpoint indicated on the abscissa. Note that not all grid points of the system have chosen to serve as new x_0 . There is a clear symmetry of the parameter regions with respect to grid point 70, which is the approximate centre of the stable 1-spot solution before the shift of x_0 .

Changing x_0 systematically over a large range of grid points, it has been observed that there are three main asymptotic spatiotemporal states: (a) uniform oscillations, (b) a single spot, (c) two spots. As mentioned, for a small set of x_0 , the spots are found to be breathing. Let us discuss the two-spot patterns: This pattern has been observed, for example, for $x_0 \in [118,131]$. This a comparatively large parameter region and shows the robustness of the pattern. Figure 5.7(a) shows a space-time plot of $|A|$ once x_0 is changed from $x_0 = 40$ to $x_0 = 118$. The transient dynamics is governed by a cascade that leads to the formation of two spots. These spots are close to each other and there is a clear increase in values of $|A|$ between the spots justifying the identification as a bound state of 2 spots, rather than a set of two independent spots. It also has been seen that the size of each spot is slightly smaller than the size of a single spot (Figure 5.2(b)). So, has been observed that a marked difference with respect to the simulation shown in Figure 5.3(b) where the two spots are well separated, each with a single-spot profile. Figure 5.7(b) shows a space-time plot of $|A|$ for a simulation with $x_0 = 147$. Now again a cascade-like behaviour in $|A|$ leading to a 2-spot pattern has been observed, however, now the distance between the spots is larger than in Figure 5.7(a) and the size of each spot is practically undistinguishable of that of a single spot (Figure 5.2(b)). When a cascade-like dynamics is observed (like routinely for a large change of x_0 like in this set of simulations), the asymptotic state cannot be easily predicted.

In Figure 5.7(c), the respective spatial profiles are shown together with the position of x_0 . It has been observed that $|A(x_0) \approx 1.45|$ in both cases and that the position of the feedback point coincides with the boundary of the spot. The different profiles of the two solutions can be interpreted in the following way: the solution in

(a) is a bound-state solution, due to the lateral interaction of the fronts limiting the spots and (b) consists of two individual spots. In spite of this difference and in order to keep the nomenclature simple, we call both patterns 2-spot solutions.

The numerical evidence collected from Figs. 5.2(b) and 5.7(c) indicates that a spot solution (of 1 or 2 spots) is found if the feedback point is located at the boundary of the spot. In the observed cases, the front profile of the spot has an oscillatory tail towards the outside region, with the feedback point being close to the maximum position of $|A|$ in the tail.

Finally, Figure 5.7(d) shows in a schematic form the asymptotic state of a simulation where x_0 has been switched from $x_0 = 40$ to another gridpoint. As mentioned above, the uniform oscillations (decay of the spot solution) have been found in, a single spot solution and a 2-spot solution, in almost perfect symmetry with respect to the centre of the 1-spot solution that represented the initial condition (grid point 70). It also shows that the asymptotic state can still be a single spot solution if the shift of the feedback point was large. In particular, there is one feedback point on either side of the spot that provides a single spot solution although in its neighbourhood the asymptotic states are uniform oscillations and 2-spot solutions. The transients for these choices of x_0 are nontrivial and small perturbations may provide large changes to the asymptotic pattern. To keep Figure 5.7(d) simple, and in particular to emphasize the symmetry with respect to grid point 70, it was decided to show data for shifts of x_0 to grid points 8 to 131. For other choices, the afore-mentioned solutions repeat, in smaller intervals.

Chapter 6

Final Remarks

Discussion

The CGLE is one of the most-studied equations in Nonlinear Dynamics and is applied to a large range of systems in the natural sciences [9]. One of its properties is that it describes an oscillatory system near a supercritical Hopf bifurcation and therefore is also a model system for nonlinear oscillations. If a reaction-diffusion system is close to a Hopf bifurcation, then spatial coupling can lead to uniform oscillations becoming unstable further to spatiotemporal chaos. Feedback methods as those studied in this thesis are known to be able to control spatiotemporal chaos in such systems. In particular, a time-delay feedback scheme with local and global contributions can suppress spatiotemporal chaos and induce regular patterns such as uniform oscillations and standing waves [13, 18, 19].

Based on these works, in this thesis, several other solutions appearing in this system have been studied. Firstly, travelling waves have been considered (Chapter 4) and secondly, spot solutions, for a slightly different model (Chapter 5).

Travelling waves have shown to be numerically transient for the chosen parameters, i.e., are unstable. Since there is no analytical study that would suggest these waves to be stable, this in itself is not critical. However, it is still surprising

since other numerical simulations [13] indicated the existence of stable travelling waves and have been found to suppress chaos in a different kind of system [34]. It has been observed in the present simulations that the transient could be longer or shorter depending on the initial condition, which may suggest that the simulations reported in [13] were simply not long enough. Nevertheless, no definite claim can be made here based on numerical evidence only.

Spot patterns are patterns that are known to exist in a variety of pattern-forming systems [35] but have not been observed in the CGLE without feedback. This is not surprising since the underlying bifurcation of the CGLE is the Hopf bifurcation and spot patterns are not generally expected near Hopf bifurcations. It was an initial hypothesis to find out whether time-delay feedback with local contributions could lead to spot patterns. As a spot pattern has a distinctive local nature, it would be surprising to find it through global feedback. Nevertheless, despite considerable effort, in the system introduced in [13], no spot patterns were found numerically.

However, by a small modification of the system, spot patterns could be created. This is the main contribution of this thesis. The modification consists of selecting a specific single point of the system to create the feedback term for the system. And the spot solution itself can be recognized by a local decrease of the modulus of the amplitude.

The pattern observed here coexists with uniform oscillations. Therefore, it can only be observed with an appropriate initial condition. The pattern was first observed as asymptotic state of a simulation that started with spatiotemporal chaos. Subsequent simulations confirmed the stability of the pattern and led us to

prepare the initial conditions to investigate the patterns systematically, showing stable 1-spot and 2-spot patterns, which furthermore confirm the local nature of the pattern. While changes of parameters or of initial conditions occasionally lead to abrupt changes in the overall dynamics (namely, via spot cascades), the stability area of spots in parameter space is not small. The stability boundaries have been found numerically with finite parameter step sizes, finite system size and finite simulation time, the location of the stability boundary is only approximate.

The pattern described in this work represents a self-organized pattern and as such its properties depend on the system parameters, as I have shown clearly through the curves that show the dependence of the spot size as function of the delay time, feedback strength and the phase shift. Its self-organized nature is also demonstrated by showing the instabilities that the pattern may undergo, namely explosion, disappearance and breathing. Small-amplitude breathing has been observed to be stable for long time intervals.

The spot is always found to be in the vicinity of the feedback point. To be precise, the feedback point is located close to the first (and highest) maximum of the amplitude of the oscillatory tail of the front representing the boundary of the spot. For a stable spot, the window of feasible feedback points to keep the spot stable is quite small (4 grid points) which corresponds to a small area around that maximum in the tail. This can be interpreted as a pinning of the spot to the neighbourhood of the feedback point.

It was decided to interpret the pattern as spot pattern, justified by the clear front-like boundary it shows in the modulus profile, in clear analogy to spot solutions in general reaction-diffusion systems [35,36]. This includes the oscillatory

(i.e., non-monotonic) tail of the front, that seems instrumental in the spot formation process, the breathing phenomenology, common for spots [35, 37, 38], and the cascading dynamics leading to transient Sierpinski-like patterns [39, 40]. The fact that a two-spot state solution can be stable, suggests that there may be n -spot patterns, if the system size is large enough. The fact that I have not observed n -spot patterns ($n > 2$) in the simulations may be due to small system size and that initial conditions should be tuned more carefully. In particular, spot cascades are frequently observed and tend to favour single spots, chaotic states or uniform oscillations as final outcome. It would be feasible to create an array of n feedback points, each with an associated area to impact on. A larger system size would be a necessary condition to observe a n -spot solution.

Two alternative interpretations of the pattern may be suggested: First, if parts of a medium are oscillating with the same oscillation frequency but with a constant phase shift, this can be interpreted as a cluster pattern (as observed, e.g., in [41]). However, the fact that the medium admits for the same parameter set 1- or 2-spot solutions suggests that the pattern is not created by a long-wavelength instability. Furthermore, the phase shift seems to be a continuous function of the system parameters and no phase-locking phenomena has been seen in my simulations.

Second, the oscillatory dynamics of the system allows for an interpretation of the pattern also as a wave sink (see [42] and references therein), i.e., an area with localized decreased oscillation frequency that asymptotically converges to a wave pattern similar to the one observed here. However, in contrast to these works, no fixed locally changed oscillation frequency was found and furthermore, the

feedback point is not located in the centre of the pattern as expected for a wave sink produced by the mechanism described in [42].

Since the feedback in this model is using the system dynamics at a single grid point, i.e., representing an area of small extension compared to the characteristic length scale, its implementation in an experimental system would be presented by a small-sized device, such as a point electrode in cardiac, neurophysiological or electrochemical systems, as long as a description of an oscillatory reaction-diffusion system is justified.

Conclusions

I can conclude that the traveling waves are numerically transient for the chosen parameters and therefore asymptotically unstable. In other work [13], the numerical simulations of the travelling waves for a different system were stable and have been found to suppress chaos. From this present work I can say that depending on the initial condition the transient of the travelling waves could be longer or shorter. This may suggest that previous numerical simulations were simply not long enough to show this kind of unstable travelling waves.

The spot pattern described in this work represents a self-organized pattern and as such its properties depend on the system parameters, as I have shown clearly through the curves that show the dependence of the spot size S as function of τ , μ and ξ . Simulations confirmed the stability of the pattern and led us to prepare the initial conditions to investigate the patterns systematically, showing stable 1-spot and 2-spot patterns, demonstrating the localized nature of the pattern. Along with cascade patterns, exploding and disappearing spots, I observe spots oscillating in size and amplitude, which show the spot's instabilities.

Outlook

Future work on this model could include a more thorough analytical description of the spot pattern including a stability analysis. This analysis should also clarify whether these spot patterns can also be expected, for example, for higher values of the delay time (in tongue-like fashion) or in spatially two-dimensional systems. Since for one-dimensional systems the feedback point is located at the spot boundary, the immediate question arises whether the same holds for two-dimensional systems and if so, if any point of the, presumably concentric, spot boundary is appropriate to create the pattern.

DC-DC power converters have been mentioned earlier in Chapter 1. Therefore, it could be interesting to compare the model presented here to the one in Ref. [44]. In principle, the model discussed here, requires to be close to a Hopf bifurcation, so a comparison with models from power converters (and possible other electronic devices) would need to take this into account. Furthermore, in the present terminology, the scheme from [44] is a global feedback as there is no spatially dependent variable, so it is quite different from the model studied in Chapter 5. Nevertheless, if there was a power electronic system with a variable that is spatially dependent (or locally coupled elements) and the possibility of addressing a single element as in this work, a comparison could be made. A possible application could be to set up a mathematical model for such a system and, in the next step, to introduce time delay feedback. One of the aims is to find out if – by optimizing delay time or feedback magnitude – the feedback can provide a way to have a steady output for a larger parameter region or being less susceptible to fluctuations, e.g., in the power input.

In power electronics – and industrial control systems in general – there already exist various types of controllers, for example PID (proportional integral derivative) controllers, that are widely used. PIDs continuously calculate the error value by differencing between the output and input voltage and applies based on proportional integral derivative terms. Thus, it could be another challenge to compare PID controllers to one based on the work presented in this thesis.

References

- [1] S. W. Smith. The Scientist and Engineer's Guide to Digital Signal Processing. *California Tech. Publishing, San Diego*, 1997.
- [2] S. Strogatz. Nonlinear Dynamics and Chaos. *Perseus Books Publishing, New York*, 1994.
- [3] J.F. De Canete, C. Galindo, and I. Garcia-Moral. Introduction to Control Systems, in: System Engineering and Automation. *Springer, Heidelberg*, 137–165, 2011.
- [4] Y.N. Kyrychko, K.B. Blyuss, S.J. Hogan, and E. Schöll. Control of spatiotemporal patterns in the Gray–Scott model. *Chaos: An Interdisciplinary Journal of Nonlinear Science*, 19(4), 2018.
- [5] W. R. Perkins. Reference Data for Engineers (Ninth Edition). *Radio, Electronics, Computer, and Communications* (2002): 15-33.
- [6] R. Hoyle. Pattern Formation, An Introduction to Methods. *Cambridge University Press*, 2006.
- [7] Diffusion, (Online accessed 12 November, 2023) Available, <https://uk.comsol.com/multiphysics/diffusion-equation>
- [8] R. A. Harvey and D. R. Ferrier. Biochemistry, *Lippincott Williams & Wilkins, Baltimore*, 2011.
- [9] I.S. Aranson, L. Kramer. The world of the complex Ginzburg-Landau equation. *Reviews of Modern Physics* 74(1):99, 2002.
- [10] A.S. Mikhailov, K. Showalter. Control of waves, patterns and turbulence in chemical systems. *Physics Reports* 425(2-3):79-194, 2006.
- [11] E. Ott, C. Grebogi, J.A. Yorke. Controlling chaos. *Physical Review Letters*, 64(11):1196, 1990.

-
- [12] K. Pyragas. Continuous control of chaos by self-controlling feedback. *Physics Letters A*, 170(6):421-428, 1992.
- [13] M. Stich, A.C. Casal, J.I. Díaz. Control of turbulence in oscillatory reaction-diffusion systems through a combination of global and local feedback. *Physical Review E*, 76(3): 036209, 2007.
- [14] D. Battogtokh, A. Mikhailov. Controlling turbulence in the complex Ginzburg-Landau equation. *Physica D: Nonlinear Phenomena*, 90(1-2):84-95, 1996.
- [15] Y.N. Kyrychko, K.B. Blyuss, S.J. Hogan, and E. Schöll. Control of spatiotemporal patterns in the Gray–Scott model. *Chaos: An Interdisciplinary Journal of Nonlinear Science*, 19(4), 2018.
- [16] O. Beck, A. Amann, E. Schöll, J.E.S. Socolar, W. Just. Comparison of time-delayed feedback schemes for spatiotemporal control of chaos in a reaction-diffusion system with global coupling. *Physical Review E*, 66(1):16213, 2002.
- [17] C. Beta, A.S. Mikhailov. Controlling spatiotemporal chaos in oscillatory reaction–diffusion systems by time-delay auto synchronization. *Physica D: Nonlinear Phenomena*, 199(1-2):173-184, 2004.
- [18] M. Stich, C. Beta. Control of pattern formation by time-delay feedback with global and local contributions. *Physica D: Nonlinear Phenomena*, 239(17):1681-1691, 2010.
- [19] M. Stich, A. Casal, C. Beta. Stabilization of standing waves through time-delay feedback. *Physical Review E*, 88(4):042910, 2013.
- [20] M. Stich. Comments on multiple oscillatory solutions in systems with time-delay feedback. *Electronic Journal of Differential Equations*, 99-109, 2015.
- [21] M. Stich, A.K. Chattopadhyay. Noise-induced standing waves in oscillatory systems with time-delayed feedback. *Physical Review E*, 93(5):052221, 2016.
- [22] K.A. Montgomery, M. Silber. Feedback control of travelling wave solutions of the complex Ginzburg–Landau equation. *Nonlinearity*, 17(6):2225, 2004.
-

-
- [23] C.M. Postlethwaite, M. Silber. Spatial and temporal feedback control of traveling wave solutions of the two-dimensional complex Ginzburg–Landau equation. *Physica D: Nonlinear Phenomena*, 236(1):65-74, 2007.
- [24] S. Boccaletti, J. Bragard. Controlling spatio-temporal chaos in the scenario of the one-dimensional complex Ginzburg–Landau equation. *Philosophical Transactions of the Royal Society A: Mathematical, Physical and Engineering Sciences*, 364(1846):2383-2395, 2006.
- [25] J. Kalantarova, T. Özsarı. Finite-parameter feedback control for stabilizing the complex Ginzburg–Landau equation. *Systems & Control Letters*, 106:40-46, 2006.
- [26] Y. Huang, H. Zhang, B. Niu. Resonant double Hopf bifurcation in a diffusive Ginzburg–Landau model with delayed feedback. *Nonlinear Dynamics*, 108(3):2223-2243, 2022.
- [27] J. C. Tzou, and S. Xie. Oscillatory translational instabilities of spot patterns in the Schnakenberg system on general 2D domains. *Nonlinearity*, 36, no. 5:2473, 2023.
- [28] Y. Nishiura and S. Xie. Dynamics of n-spot rings with oscillatory tails in a three-component reaction-diffusion system. *SIAM Journal on Applied Dynamical Systems*, 21, no. 3:2268-2296, 2022.
- [29] L. Yang and I. R. Epstein. Oscillatory Turing patterns in reaction-diffusion systems with two coupled layers. *Physical review letters*, 90, no. 17:178303, 2003.
- [30] F. Al Saadi, A. Champneys, A. Worthy, and A. Msmali. Stationary and oscillatory localized patterns in ratio-dependent predator–prey systems. *IMA Journal of Applied Mathematics*, 86, no. 4:808-827, 2021.
- [31] T. Ohta. Pulse dynamics in a reaction–diffusion system. *Physica D: Nonlinear Phenomena*, 151, no. 1:61-72, 2001.
- [32] T. Ohta, and J. Kiyose. Collision of domain boundaries in a reaction-diffusion system. *Journal of the Physical Society of Japan*, 65, no. 7:1967-1970, 1996.
-

-
- [33] C. B. Muratov and V. V. Osipov. Static spike autosolitons in the Gray-Scott model. *Journal of Physics A: Mathematical and General*, 33, no. 48:8893, 2000.
- [34] Y.N. Kyrychko, K.B. Blyuss, S.J. Hogan, and E. Schöll. Control of spatiotemporal patterns in the Gray-Scott model. *Chaos: An Interdisciplinary Journal of Nonlinear Science*, 19, no. 4, 043126, 2009.
- [35] A. S. Mikhailov. Foundations of Synergetics I, 2nd Edition, *Springer*, Berlin, 1994.
- [36] M. Stich, G. Ghoshal, and J. Pérez-Mercader. Parametric pattern selection in a reaction-diffusion model. *PLoS ONE*, 8, no. 10, e77337, 2003.
- [37] T. Ohta, and J. Kiyose. Collision of domain boundaries in a reaction-diffusion system. *Journal of the Physical Society of Japan*, 65(7), pp.1967-1970, 1996.
- [38] D. Haim, G. Li, Q. Ouyang, W.D. McCormick, H.L. Swinney, A. Hagberg, E. Meron. Breathing spots in a reaction-diffusion system. *Physical Review Letters* 77, no. 1, p190, 1996.
- [39] Y. Hayase, T. Ohta. Sierpinski gasket in a reaction-diffusion system. *Physical Review Letters* 81, no. 8, 1726, 1998.
- [40] H. Chaté, H., A. Pikovsky, and O. Rudzick. Forcing oscillatory media: phase kinks vs. synchronization. *Physica D: Nonlinear Phenomena*, 131(1-4), pp.17-30, 1999.
- [41] D. Battogtokh, A. Preusser, and A. Mikhailov. Controlling turbulence in the complex Ginzburg-Landau equation II. Two-dimensional systems. *Physica D: Nonlinear Phenomena*, 106(3-4), pp.327-362, 1997.
- [42] M. Stich, A. S. Mikhailov. Complex pacemakers and wave sinks in heterogeneous oscillatory chemical systems. *Zeitschrift für Physikalische Chemie* 216, 521, 2002.
- [43] J. Deane. Chaos in a Current-Mode Controlled Boost DC-DC Converter. *IEEE Transactions on Circuits and Systems 1: Fundamental Theory and Applications*, 39 (8), 680-683, 1992.
-

- [44] A.N. Natsheh, N.B. Janson, J.G. Kettleborough. Control of Chaos in a DC-DC Boost Converter. *IEEE International Symposium on Industrial Electronics*, 2008.

Appendix

Real and imaginary parts of the CGLE with local and global feedback

The CGLE with local and global feedback is written as

$$\frac{\partial A}{\partial t} = (1 - i\omega)A - (1 + i\alpha)|A|^2A + (1 + i\beta)\frac{\partial^2 A}{\partial x^2} + F$$

where, A = complex oscillation amplitude

ω = linear frequency parameter

α = nonlinear frequency parameter

β = linear dispersion coefficient

F = feedback term

$$F = \mu \cdot e^{i\xi} \cdot [m_l\{A(x, t - \tau) - A(x, t)\} + m_g\{\bar{A}(t - \tau) - \bar{A}(t)\}]$$

where, μ = feedback strength

ξ = phase shift

τ = time delay

m_g = global feedback

m_l = local feedback

and $\bar{A}(t) = \frac{1}{L} \int_0^L A(x, t) dx$

where, \bar{A} = spatial average

L = one-dimensional system length

Replace, $A = a + ib$

$$\text{L.H.S.} = \frac{\partial A}{\partial t} = \frac{\partial(a+ib)}{\partial t} = \frac{\partial a}{\partial t} + i \frac{\partial b}{\partial t}$$

(non-spatial part)

$$\begin{aligned} \text{R.H.S.} &= (1 - i\omega)(a + ib) - (1 + i\alpha)|a + ib|^2(a + ib) \\ &= (a + ib - ia\omega + \omega b) - (a + ib + ia\alpha - \alpha b)|a + ib|^2 \\ &= (a + ib - ia\omega + \omega b) - (a + ib + ia\alpha - \alpha b)(a^2 + ib^2)(a^2 - ib^2) \\ &= (a + ib - ia\omega + \omega b) - (a + ib + ia\alpha - \alpha b)(a^2 + b^2) \\ &= (a + ib - ia\omega + \omega b) - (a^3 + a^2ib + ia^3\alpha - a^2b\alpha + ab^2 + ib^3 + iab^2\alpha - \alpha b^3) \\ &= a + ib - ia\omega + \omega b - a^3 - a^2ib - ia^3\alpha + a^2b\alpha - ab^2 - ib^3 - iab^2\alpha + \alpha b^3 \\ &= \{a - a^3 - ab^2 + \omega b + a^2b\alpha + \alpha b^3\} + i\{b - a^2b - b^3 + \omega a + a^3\alpha - ab^2\alpha\} \\ &= [a\{1 - (a^2 + b^2)\} + \omega b + b\alpha(a^2 + b^2)] + i\{b\{1 - (a^2 + b^2)\} - \omega a - a\alpha(a^2 + b^2)\} \end{aligned}$$

(Laplacian)

$$\begin{aligned} \text{R.H.S.} &= (1 + i\beta)\nabla^2 A \\ &= (1 + i\beta)\nabla^2(a + ib) \\ &= (1 + i\beta)\left\{\frac{\partial^2 a}{\partial x^2} + i\frac{\partial^2 b}{\partial x^2}\right\} \\ &= \frac{\partial^2 a}{\partial x^2} + i\frac{\partial^2 b}{\partial x^2} + i\beta\frac{\partial^2 a}{\partial x^2} - \beta\frac{\partial^2 b}{\partial x^2} \\ &= \frac{\partial^2 a}{\partial x^2} - \beta\frac{\partial^2 b}{\partial x^2} + i\left\{\beta\frac{\partial^2 a}{\partial x^2} + \frac{\partial^2 b}{\partial x^2}\right\} \\ &= \frac{\partial^2}{\partial x^2}(a - \beta b) + i\frac{\partial^2}{\partial x^2}(\beta a + b) \end{aligned}$$

(Feedback)

$$\begin{aligned} \text{R.H.S.} &= \mu \cdot e^{i\xi} \cdot [m_l\{A(x, t - \tau) - A(x, t)\} + m_g\{\bar{A}(t - \tau) - \bar{A}(t)\}] \\ &= \mu \cdot e^{i\xi} \cdot [m_l\{a(x, t - \tau) + i \cdot b(x, t - \tau) - a(x, t) - i \cdot b(x, t)\} + m_g\{\bar{A}(t - \tau) - \bar{A}(t)\}] \end{aligned}$$

$$\begin{aligned}
\bar{A}(t) &= \frac{1}{L} \int_0^L A(x, t) dx \\
&= \frac{1}{L} \int_0^L a(x, t) dx + i \cdot \frac{1}{L} \int_0^L b(x, t) dx \\
&= \bar{a}(x, t) + i \cdot \bar{b}(x, t)
\end{aligned}$$

$$\begin{aligned}
\bar{A}(t - \tau) &= \frac{1}{L} \int_0^L A(x, t - \tau) dx \\
&= \frac{1}{L} \int_0^L a(x, t - \tau) dx + i \cdot \frac{1}{L} \int_0^L b(x, t - \tau) dx \\
&= \bar{a}(x, t - \tau) + i \cdot \bar{b}(x, t - \tau)
\end{aligned}$$

$$\begin{aligned}
\therefore F &= \mu \cdot e^{i\xi} \cdot [m_l \{a(x, t - \tau) + i \cdot b(x, t - \tau) - a(x, t) - i \cdot b(x, t)\} \\
&\quad + m_g \{\bar{a}(x, t - \tau) + i \cdot \bar{b}(x, t - \tau) - \bar{a}(x, t) - i \cdot \bar{b}(x, t)\}]
\end{aligned}$$

From Euler's formula,

$$e^{i\xi} = \cos \xi + i \cdot \sin \xi$$

$$\begin{aligned}
\therefore F &= \mu \cdot (\cos \xi + i \cdot \sin \xi) \\
&\quad \cdot [m_l \{a(x, t - \tau) + i \cdot b(x, t - \tau) - a(x, t) - i \cdot b(x, t)\} \\
&\quad + m_g \{\bar{a}(x, t - \tau) + i \cdot \bar{b}(x, t - \tau) - \bar{a}(x, t) - i \cdot \bar{b}(x, t)\}] \\
&= \mu \cdot [m_l \cdot (\cos \xi + i \cdot \sin \xi) \\
&\quad \cdot \{a(x, t - \tau) + i \cdot b(x, t - \tau) - a(x, t) - i \cdot b(x, t)\} + m_g \\
&\quad \cdot (\cos \xi + i \cdot \sin \xi) \\
&\quad \cdot \{\bar{a}(x, t - \tau) + i \cdot \bar{b}(x, t - \tau) - \bar{a}(x, t) - i \cdot \bar{b}(x, t)\}] \\
&= \mu \cdot [(m_l \cdot \cos \xi + i \cdot m_l \cdot \sin \xi) \\
&\quad \cdot \{a(x, t - \tau) + i \cdot b(x, t - \tau) - a(x, t) - i \cdot b(x, t)\} \\
&\quad + (m_g \cdot \cos \xi + i \cdot m_g \cdot \sin \xi) \\
&\quad \cdot \{\bar{a}(x, t - \tau) + i \cdot \bar{b}(x, t - \tau) - \bar{a}(x, t) - i \cdot \bar{b}(x, t)\}]
\end{aligned}$$

$$\begin{aligned}
&= \mu \cdot [a(x, t - \tau) \cdot m_l \cdot \cos \xi + i \cdot b(x, t - \tau) \cdot m_l \cdot \cos \xi - a(x, t) \cdot m_l \cdot \cos \xi \\
&\quad - i \cdot b(x, t) \cdot m_l \cdot \cos \xi + a(x, t - \tau) \cdot i \cdot m_l \cdot \sin \xi + i^2 \\
&\quad \cdot b(x, t - \tau) \cdot m_l \cdot \sin \xi - a(x, t) \cdot i \cdot m_l \cdot \sin \xi - i^2 \cdot b(x, t) \\
&\quad \cdot m_l \cdot \sin \xi + \bar{a}(x, t - \tau) \cdot m_g \cdot \cos \xi + i \cdot \bar{b}(x, t - \tau) \cdot m_g \cdot \cos \xi \\
&\quad - \bar{a}(x, t) \cdot m_g \cdot \cos \xi - i \cdot \bar{b}(x, t) \cdot m_g \\
&\quad \cdot \cos \xi + \bar{a}(x, t - \tau) \cdot i \cdot m_g \cdot \sin \xi + i^2 \cdot \bar{b}(x, t - \tau) \cdot m_g \cdot \sin \xi \\
&\quad - \bar{a}(x, t) \cdot i \cdot m_g \cdot \sin \xi - i^2 \cdot \bar{b}(x, t) \cdot m_g \cdot \sin \xi] \\
&= \mu \cdot [a(x, t - \tau) \cdot m_l \cdot \cos \xi + i \cdot b(x, t - \tau) \cdot m_l \cdot \cos \xi - a(x, t) \cdot m_l \cdot \cos \xi \\
&\quad - i \cdot b(x, t) \cdot m_l \cdot \cos \xi + a(x, t - \tau) \cdot i \cdot m_l \cdot \sin \xi - b(x, t - \tau) \\
&\quad \cdot m_l \cdot \sin \xi - a(x, t) \cdot i \cdot m_l \cdot \sin \xi + b(x, t) \cdot m_l \cdot \sin \xi \\
&\quad + \bar{a}(x, t - \tau) \cdot m_g \cdot \cos \xi + i \cdot \bar{b}(x, t - \tau) \cdot m_g \cdot \cos \xi - \bar{a}(x, t) \\
&\quad \cdot m_g \cdot \cos \xi - i \cdot \bar{b}(x, t) \cdot m_g \\
&\quad \cdot \cos \xi + \bar{a}(x, t - \tau) \cdot i \cdot m_g \cdot \sin \xi - \bar{b}(x, t - \tau) \cdot m_g \cdot \sin \xi \\
&\quad - \bar{a}(x, t) \cdot i \cdot m_g \cdot \sin \xi + \bar{b}(x, t) \cdot m_g \cdot \sin \xi] \\
&= \mu \cdot [a(x, t - \tau) \cdot m_l \cdot \cos \xi - a(x, t) \cdot m_l \cdot \cos \xi - b(x, t - \tau) \cdot m_l \cdot \sin \xi \\
&\quad + b(x, t) \cdot m_l \cdot \sin \xi - \bar{a}(x, t) \cdot m_g \cdot \cos \xi - \bar{b}(x, t - \tau) \\
&\quad \cdot m_g \cdot \sin \xi + \bar{a}(x, t - \tau) \cdot m_g \cdot \cos \xi + \bar{b}(x, t) \cdot m_g \cdot \sin \xi \\
&\quad + i \{ b(x, t - \tau) \cdot m_l \cdot \cos \xi - b(x, t) \cdot m_l \cdot \cos \xi + a(x, t - \tau) \\
&\quad \cdot m_l \cdot \sin \xi - a(x, t) \cdot m_l \cdot \sin \xi + \bar{b}(x, t - \tau) \cdot m_g \cdot \cos \xi - \bar{b}(x, t) \\
&\quad \cdot m_g \cdot \cos \xi + \bar{a}(x, t - \tau) \cdot m_g \cdot \sin \xi - \bar{a}(x, t) \cdot m_g \cdot \sin \xi \}] \\
&= \mu \cdot a(x, t - \tau) \cdot m_l \cdot \cos \xi - \mu \cdot a(x, t) \cdot m_l \cdot \cos \xi - \mu \cdot b(x, t - \tau) \\
&\quad \cdot m_l \cdot \sin \xi + \mu \cdot b(x, t) \cdot m_l \cdot \sin \xi - \mu \cdot \bar{a}(x, t) \cdot m_g \cdot \cos \xi - \mu \\
&\quad \cdot \bar{b}(x, t - \tau) \cdot m_g \cdot \sin \xi + \mu \cdot \bar{a}(x, t - \tau) \cdot m_g \cdot \cos \xi + \mu \cdot \bar{b}(x, t) \\
&\quad \cdot m_g \cdot \sin \xi \\
&\quad + i \{ \mu \cdot b(x, t - \tau) \cdot m_l \cdot \cos \xi - \mu \cdot b(x, t) \cdot m_l \cdot \cos \xi + \mu \\
&\quad \cdot a(x, t - \tau) \cdot m_l \cdot \sin \xi - \mu \cdot a(x, t) \cdot m_l \cdot \sin \xi + \mu \cdot \bar{b}(x, t - \tau) \\
&\quad \cdot m_g \cdot \cos \xi - \mu \cdot \bar{b}(x, t) \cdot m_g \\
&\quad \cdot \cos \xi + \mu \cdot \bar{a}(x, t - \tau) \cdot m_g \cdot \sin \xi - \mu \cdot \bar{a}(x, t) \cdot m_g \cdot \sin \xi \}
\end{aligned}$$

$$\begin{aligned}
&= \mu \cdot a(x, t - \tau) \cdot m_l \cdot \cos \xi - \mu \cdot a(x, t) \cdot m_l \cdot \cos \xi - \mu \cdot \bar{a}(x, t) \cdot m_g \cdot \cos \xi \\
&\quad + \mu \cdot \bar{a}(x, t - \tau) \cdot m_g \cdot \cos \xi - \mu \cdot b(x, t - \tau) \cdot m_l \cdot \sin \xi + \mu \\
&\quad \cdot b(x, t) \cdot m_l \cdot \sin \xi - \mu \cdot \bar{b}(x, t - \tau) \cdot m_g \cdot \sin \xi + \mu \cdot \bar{b}(x, t) \\
&\quad \cdot m_g \cdot \sin \xi \\
&\quad + i \{ \mu \cdot b(x, t - \tau) \cdot m_l \cdot \cos \xi - \mu \cdot b(x, t) \cdot m_l \cdot \cos \xi + \mu \\
&\quad \cdot \bar{b}(x, t - \tau) \cdot m_g \cdot \cos \xi - \mu \cdot \bar{b}(x, t) \cdot m_g \cdot \cos \xi + \mu \cdot a(x, t - \tau) \\
&\quad \cdot m_l \cdot \sin \xi - \mu \cdot a(x, t) \cdot m_l \cdot \sin \xi + \mu \cdot \bar{a}(x, t - \tau) \cdot m_g \cdot \sin \xi \\
&\quad - \mu \cdot \bar{a}(x, t) \cdot m_g \cdot \sin \xi \} \\
&= \mu \cdot \cos \xi \cdot [m_l \cdot \{a(x, t - \tau) - a(x, t)\} + m_g \cdot \{\bar{a}(x, t - \tau) - \bar{a}(x, t)\}] - \mu \\
&\quad \cdot \sin \xi \\
&\quad \cdot [m_l \cdot \{b(x, t - \tau) - b(x, t)\} + m_g \cdot \{\bar{b}(x, t - \tau) - \bar{b}(x, t)\}] \\
&\quad + i \{ \mu \cdot \cos \xi \\
&\quad \cdot [m_l \cdot \{b(x, t - \tau) - b(x, t)\} + m_g \cdot \{\bar{b}(x, t - \tau) - \bar{b}(x, t)\}] \\
&\quad + \mu \cdot \sin \xi \\
&\quad \cdot [m_l \cdot \{a(x, t - \tau) - a(x, t)\} + m_g \cdot \{\bar{a}(x, t - \tau) - \bar{a}(x, t)\}] \}
\end{aligned}$$

Summarizing:

Real Part: $\frac{\partial a}{\partial t} = a\{1 - (a^2 + b^2)\} + b\{\omega + \alpha(a^2 + b^2)\} +$
 $\frac{\partial^2}{\partial x^2}(a - \beta b) + \mu \cdot \cos \xi \cdot [m_l \cdot \{a(x, t - \tau) - a(x, t)\} + m_g \cdot \{\bar{a}(x, t - \tau) -$
 $\bar{a}(x, t)\}] - \mu \cdot \sin \xi \cdot [m_l \cdot \{b(x, t - \tau) - b(x, t)\} + m_g \cdot \{\bar{b}(x, t - \tau) -$
 $\bar{b}(x, t)\}]$

Imaginary Part: $\frac{\partial b}{\partial t} = b\{1 - (a^2 + b^2)\} + a\{\omega + \alpha(a^2 + b^2)\} +$
 $\frac{\partial^2}{\partial x^2}(\beta a + b) + \mu \cdot \cos \xi \cdot [m_l \cdot \{b(x, t - \tau) - b(x, t)\} + m_g \cdot \{\bar{b}(x, t - \tau) -$
 $\bar{b}(x, t)\}] + \mu \cdot \sin \xi \cdot [m_l \cdot \{a(x, t - \tau) - a(x, t)\} + m_g \cdot \{\bar{a}(x, t - \tau) -$
 $\bar{a}(x, t)\}]$
